PETRA III extension project

Beamlines P64 / P65
for X-ray absorption spectroscopy

Technical design report

Final version Oct. 09, 2012

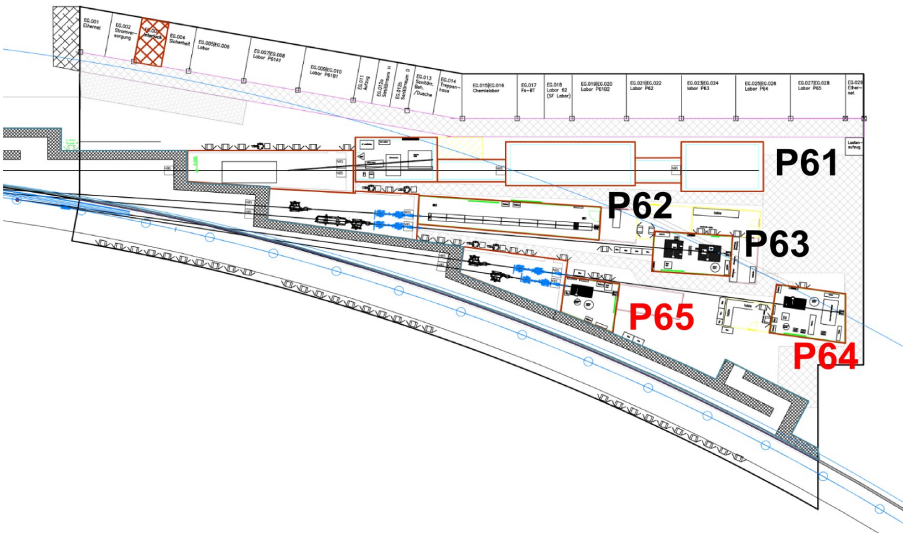

Contributors

DESY Photon Science (FS-DO)

Wolfgang Caliebe	Workpackage Leader P64
Michael Murphy	Postdoc P64
Ulf Brüggmann	Beamline Engineer P64
Edmund Welter	Workpackage Leader P65
Roman Chernikov	Postdoc P65
Mathias Herrmann	Beamline Engineer P65
Wolfgang Drube	PETRA III Extension Project Leader
Martin Tolkiehn	Workpackage Leader P24
	Data Acquisition Electronics for the 100-element Detector

University of Wuppertal, Physics Department

BMBF funded project for the implementation of a QEXAFS Monochromator at P64

Ronald Frahm	Project Leader
Dirk Lützenkirchen–Hecht	Senior scientist
Oliver Müller	PhD student

University of Paderborn, Chemistry Department

BMBF funded project "BioXAS at PETRA III" including special sample environments and partial funding for a 100-element Ge-Detector for P64

Gerald Henkel	Project Leader

This technical design has been iterated several times with numerous colleagues from FS, and we particularly acknowledge fruitful discussions with many experts from the beamline technology group (FS-BT), undulator systems group (FS-US), and the technical infrastructure group (FS-TI).

1 Introduction

DESY is one of the world's leading accelerator centres and a member of the Helmholtz Association. It develops, builds and operates large particle accelerators used to investigate the structure of matter. Photon science is a major branch of its research activities and DESY has a long standing tradition in the use of synchrotron radiation. For over 30 years, the 2^{nd} generation facility DORIS III served as a very productive high-flux source for synchrotron radiation based research. Currently, the main photon sources are the storage ring PETRA III and the Free-Electron-Laser FLASH, offering unique research possibilities for an international scientific community.

PETRA III is a low-emittance (1 nmrad) 6 GeV storage ring resulting from the conversion of the large PETRA accelerator into a 3^{rd} generation light source. This project started in 2007, and the first beamlines became operational in 2009. Today, a total of 14 undulator beamlines are in operation in a large experimental hall covering 1/8 of the storage ring.

The focus of the new facility is on applications making optimum use of the high beam brilliance, i.e. experiments aiming at nano focusing, ultra-high resolution studies and coherence applications. Other techniques which require photon flux but not ultimate brilliance are being continued very successfully at DORIS III which is operated in parallel to PETRA III sharing its chain of pre-accelerators.

1.1 PETRA III Extension Project

It has been decided to shut down the DORIS III facility at the end of 2012. However, some very productive DORIS III beamlines and instruments cover techniques which are not currently implemented at PETRA III. In order to carry on these activities and to provide competitive beamlines and instrumentation for these applications, the experimental facilities at PETRA III will be extended to provide additional beamlines.

This PETRA III extension project comprises two new experimental halls on either side of the large new PETRA III hall (North and East) making use of the long straight sections and the adjacent arcs (see figure 1).

The northern straight section already accommodates one of the 40 m long damping wiggler arrays producing an extremely hard and powerful X-ray beam which can also be utilized for experiments. The long straight in the east is available for additional insertion devices.

In order to provide additional sources also in the corresponding arc sections, which currently are filled by long dipole magnets yielding a rather soft spectrum, the machine lattice will be modified in either arc. The new lattice comprises two double bent achromat (DBA) cells each providing a 5 m long straight section. Similar to the present PETRA III beamlines,

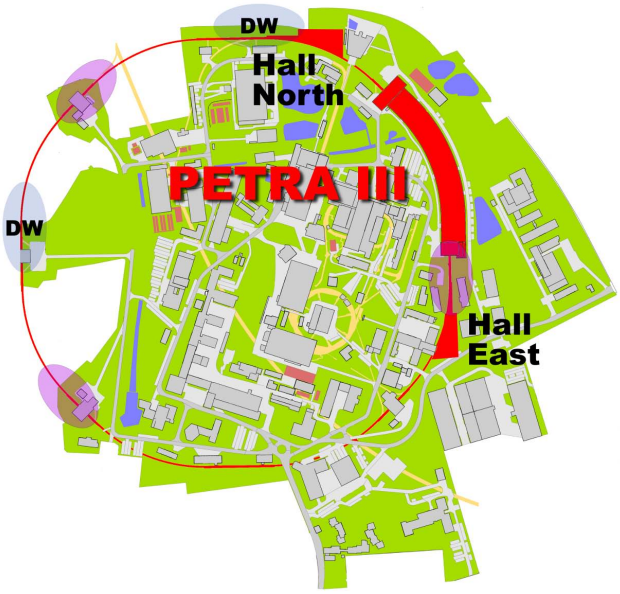

Figure 1: View of the PETRA III storage ring (red line) showing the present experimental hall together with the planned additional experimental halls in the North and East.

these straights will serve two beamlines independently by use of canting dipoles resulting in two separate 2 m straights. The canting angle was chosen to be 20 mrad in order to provide sufficient spatial flexibility for the experiments further downstream. In total, the new lattice provides eight short straight sections in the two arcs with identical source properties which are very similar to a current high-β section at PETRA III making them very suitable for the use of undulators. In total 10 new beamlines will be built which will be up to 140 m long.

Five of the new beamlines will be designed as "mini undulator" beamlines continuing most of the productive DORIS III techniques. The number of magnet poles will be adapted to match the tolerable power load on the well-performing DORIS bending magnet monochromators which - in the beginning - will be re-used. These sources will not only be very well suited for the spectrum of applications to be relocated from DORIS III but also provide a considerably brighter beam. In addition, four additional high-brilliance undulator beamlines will be built, three in collaboration with international partners, Sweden, India and Russia. One beamline will make use of the hard X-ray spectrum from the 40 m long damping wiggler array already present in the North. Because of the large machine radius, bending magnets are not available as X-ray photon sources.

Since 2009, the specification of the techniques to be implemented are being discussed with the user community, scientific advisory bodies and international partners. A number of specific user workshops have been held. The compilation of beamlines and techniques resulting from this discussion is summarized in table 1.

A critical issue is the timing of the construction of the extension project because its realization requires a complete shutdown of the current PETRA III user facility for an extended

Table 1: Beamlines and techniques in the PETRA III extension halls East and North.

PETRA III East			
beamline	**applications / instruments**	**insertion device**	**range**
P21	Swedish materials science beamline - high-energy in-situ X-ray diffraction and scattering for materials science research - large sample imaging	4 m undulator & wiggler	~50-200 keV
P22	nano X-ray spectroscopy (India-DESY collaboration) applications (to be discussed)	2 m undulator	~3-50 keV
P23	nano X-ray diffraction (Russian-German collaboration) - structure & processes in low-dimensional and nanoscale systems) - (time-resolved) nano-diffraction in complex and in-situ sample environments - low-T, high-pressure diffraction	2 m undulator	~5-50 keV
P24	chemical crystallography - single-crystal diffraction - pump-probe diffraction techniques - diffuse scattering - low temperature & non-ambient sample environments	mini-undulator	~8-40 keV
P25	P25.1 education/training/testing (to be discussed) P25.2 fixed energy side-branch (to be discussed)	mini-undulator	to be discussed
PETRA III North			
P61	P61.1 fixed-energy side branch (tentative: PDF instrument; feasibility study ongoing) ; P61.2a high-energy engineering materials science station (Helmholtz-Centre Geesthacht, HZG) P61.2b extreme conditions (large volume press)	damping wiggler (40 m)	~50-200 keV monochr. & pink beam
P62	small angle X-ray scattering WAXS, SAXS, USAXS in transmission & reflection geometry with moderate beamsize	mini-undulator	~10-25 keV
P63	X-ray micro fluorescence micro-probe applications beam size down to ~5 μm^2	mini-undulator	~3-45 keV
P64	X-ray absorption spectroscopy time-resolved studies & diluted systems bio-XAFS	2 m undulator	~4-45 keV
P65	X-ray absorption spectroscopy in-situ studies for catalysis & chemistry	mini-undulator	~4-45 keV

period of time. Also, a priorization of the new beamlines has to be defined because they cannot be built in parallel. A further complication arises because of the DORIS III shutdown end of 2012 which will discontinue the availability of some important techniques at DESY.

X-ray absorption spectroscopy is one of the key techniques at DORIS III, and no suitable alternative is currently available at PETRA III. It was therefore discussed and decided to build two new XAFS beamines (P64 and P65) at the PETRA III extension to continue these productive and successful activities.

The science case was discussed in several user workshops and to a large extent is a continuation of the current activities. New aspects arise, however, because of the much higher source brilliance. It was decided to build one of the XAFS beamlines (P64) for flux limited applications such as time-resolved studies using QEXAFS and diluted systems in bioXAFS. This beamline will be equipped with a full length insertion device. In terms of beamline priorization, there is broad consensus that the two XAFS beamlines will be built first.

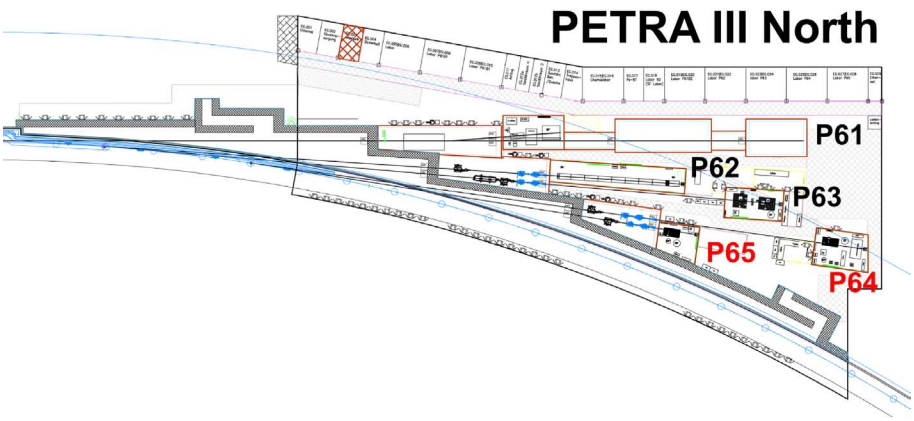

Figure 2: Floor plan of the beamline arrangement in the Northern hall (P61-P65) of the PETRA III extension. P64 and P65 are the new XAFS beamlines.

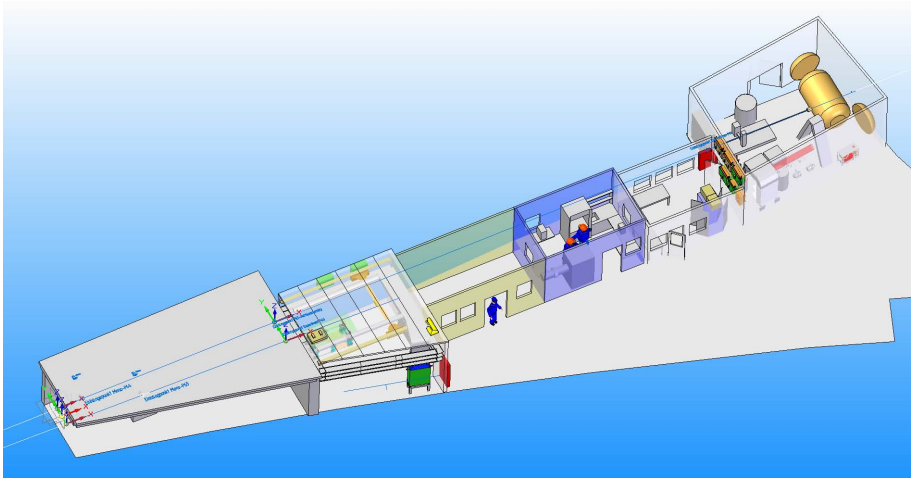

Figure 3: CAD drawing of P64/65 (sector 3 of hall north)

According to the current schedule, the civil construction of the PETRA III extension will start May 13, 2013. During the machine modifications and the initial construction phase of the experimental halls, the storage ring cannot be operated and the user operation at PETRA III will pause. Every effort will be made to minimize this interruption. After the machine restart in October 2013, the completion of the new facilities PETRA III North and East will continue in parallel. It is planned that the XAFS beamlines in PETRA III North (see figure 3) will be available for experiments in fall 2014.

This technical design report describes the basic functions of the beamlines, as they should be available in the first year of operations. Some features will not be available right on the first day of user operation, but they will be implemented within the following months. Several additional features like lower or higher photon energies, or a high energy-resolution x-ray emission spectrometer can be added in the following years, if there is a justified user demand.

1.2 XAFS User Workshops

The science case along with suitable design parameters were discussed with the user community of the DORIS III EXAFS beamlines in two workshops which took place in 2010 and 2011.

It was general consensus that the two new beamlines should on the one hand allow a continuation of the very successful work done at DORIS III XAFS beamlines (A1, C, X1) and that on the other hand they should make use of the superior properties of the PETRA III source to improve and extend the range of applications by novel methods, which so far were limited due to beam properties at DORIS III. Among these are time-resolved measurements (QEXAFS) in the 10 Hz and faster range, studies of highly-diluted systems, and wave-length dispersive spectrometers for a better separation of fluorescence lines compared to energy-dispersive solid-state detectors. The obvious way to realise these partly conflicting demands is to focus the properties of one of the beamlines on standard XAFS experiments with a relatively large beam and moderate flux density and to use the second beamline for more advanced experimental methods.

Also, it was noted that XAFS using synchrotron radiation is a very powerful technique being applied in many different fields of science such as physics, chemistry, biology, environmental sciences, cultural heritage, etc. Many users, especially less-experienced and new users, would like to use XAFS for routine measurements in a way similar to laboratory methods. However, many of the newer XAFS beamlines nowadays focus on small spot sizes and high photon flux. These beamlines are often not well suited for routine XAFS measurements, also due to their increased complexity. Ease of use and robustness is therefore also seen as a key requirement for the new beamlines at the PETRA III extension.

The intention of beamline P65 is to provide a new "workhorse beamline" with enhanced capabilities for the existing large DORIS III user community. The largest fraction of users of the existing beamline focus on applications in chemistry, especially catalytic chemistry. The requested beamline parameters as discussed in the user workshops are:

- Energy range 4-45 keV, covering the K or L3 absorption edges of relevant elements
- Energy resolution intrinsic to Si(111) or Si(311)
- Large (1 - 2 mm^2) beam
- Infrastructure for in-situ applications
- Photon flux of $10^{10}\,s^{-1}$ – $10^{11}\,s^{-1}$
- Easy operation also for novel and less experienced user groups

Beamline P64 will be optimised for flux-hungry applications like QEXAFS in the 10 Hz-range and faster, spectroscopy of highly-diluted systems, and resonant x-ray emission spectroscopy (RXES).

- Energy range 4-45 keV, covering the K or L3 absorption edges of the relevant elements
- Energy resolution intrinsic to Si(111) or Si(311)
- Beamsize (0.01 mm^2) beam
- Infrastructure for in-situ applications
- Photon flux $> 10^{12}\,s^{-1}$
- 2 DCMs, DESY high heat load DCM and special Q-EXAFS DCM
- Spectrometer for RXES etc.
- Easy operation also for novel and less experienced user groups

The main target of QEXAFS will be in-operando experiments of catalytic reactions. Currently, such experiments are limited at DORIS III beamlines by the incident flux to the minute time-scale. In order to acquire complete XAFS scans on the 0.1 s time-scale, at least 10^{12} photon/s are required. This is not feasible at a DORIS III bending magnet beamline, but will certainly be possible at a PETRA III insertion device beamline. Highly-diluted systems like proteins suffer also from the rather low flux at DORIS III bending magnets. In some instances, it is not possible to get more sample material in order to increase the signal. These systems will profit significantly from a 3-4 orders of magnitude larger flux, which can be obtained from a PETRA III insertion device. Finally, RXES requires good energy resolution and high flux in order to gain additional information on the near-edge structure. This combination cannot be obtained even at a DORIS III wiggler beamline due to the rather large vertical source size. Due to the high source brilliance at PETRA III, high energy resolution will be available with high photon flux.

This TDR will present both beamlines, P64 and P65. In the following, the specific source properties of both beamlines will be discussed together, because the technical challenges are very similar. Thereafter, the concepts and technical design as well as expected applications and performances of beamlines P64 and P65 will be presented and discussed in separate chapters.

2 The Source

The following conditions have to be fulfilled by the source for an EXAFS-beamline:

- Continuous energy range 4 - 45 keV
- Uniform intensity distribution of the beamprofile
- Rather constant flux with intensity variations less than a factor of 2 over the entire energy range of an EXAFS-scan (about 1 - 2 keV)
- High flux: 10^{12} ph/s for QEXAFS (at least 10^7 ph within the measuring interval).

Several boundary conditions also have an influence on the performance of the EXAFS-beamline, which have to be considered for the choice of the optimum source:

- The first optical component can be installed at a distance of 53 m from the source and not closer.
- The white-beam slits have a maximum opening of 10 mm in the horizontal and 6 mm in the vertical direction. It is not possible to move the center of the slits and keep this maximum opening constant. The installation error is of the order of 100 μm. The white beam slits are installed about 45 m downstream of the source.
- The total power of the source cannot exceed 10 kW, and the maximum on-axis power density has to be less than 200 kW/mrad^2. This limitation is given by the existing front-end components and by the high heat-load monochromator. The maximum power-density for the existing C-type monochromator cannot exceed 2 W/mm^2.

The choice of the optimum radiation source for an EXAFS-beamline is a rather difficult task. The following possibilities exist:

1. Bending magnet
2. Wiggler
3. Undulator

In the following sections, we will discuss the main properties of these devices with respect to EXAFS, in order to make the best selection.

2.1 Bending Magnet

A bending magnet is the most simple source for synchrotron radiation. It emits radiation with a vertical opening angle of $1/\gamma$ at the critical energy. This opening angle decreases with energy. The horizontal opening angle corresponds to the deflection angle of the bending magnet. The energy spectrum depends on the magnetic field strength. The existing bending magnets of the FODO-lattice in the old octants are rather long (5.1 m) and have a weak field, why their critical energy is rather low with E_c=2.1 keV. This is too low for the desired energy range, however, it is possible to replace these magnets with shorter ones, which have a higher field. The bending magnets between two DBA-cells of the new octant have a critical energy of about 17 keV, which would be well suited for an EXAFS beamline. Such a device has a higher brilliance than a bending magnet at DORIS III. However, the beamlines at PETRA III are rather long compared to DORIS III. In order to collect a horizontal divergence of 2 mrad at a distance of about 50 m, which is the closest position of optical components to the ring, they have to have a width of more than 100 mm. This might be feasible for a monochromator, however, it is not practical for mirrors, which have a sagittal radius of the order of 120 mm. Therefore, the flux of a bending magnet beamline at PETRA III will not be higher than that of an existing bending magnet beamline at DORIS III. Besides, space limitations in the experimental hall do not allow for additional bending magnet beamlines in between ID beamlines.

2.2 Wiggler

In the conventional picture, a wiggler is the incoherent superposition of radiation from separate bending magnets. This simplifying picture is true for the conventional x-ray range (>8 keV) at low energy machines with normal emittance. However, this picture fails even at a machine like DORIS III with a horizontal emittance of 410 nmrad for the soft x-ray range, where the W1-wiggler behaves like an undulator. At least the first harmonic is clearly visible, and the gap has to be tuned for optimum performance in the soft x-ray range. At a high-energy machine like PETRA III with very low emittance, the simple picture fails even in the conventional x-ray range. Calculations with Spectra (Tanaka & Kitamura, 2001) indicate that narrow harmonics with a width of 50 eV are still visible at energies higher than 8 keV (see figure 4). If we chose a wiggler with a larger K-value in order to push these high harmonics closer together, we will increase the total heatload on the front-end components to unacceptable values. The existing front-end components can only tolerate a wiggler up to K$\simeq$5.

In addition to the high heatload, the intensity distribution of a medium-K wiggler is rather inhomogeneous, and it varies with energy (see figures 5 and 6). A wiggler at PETRA III

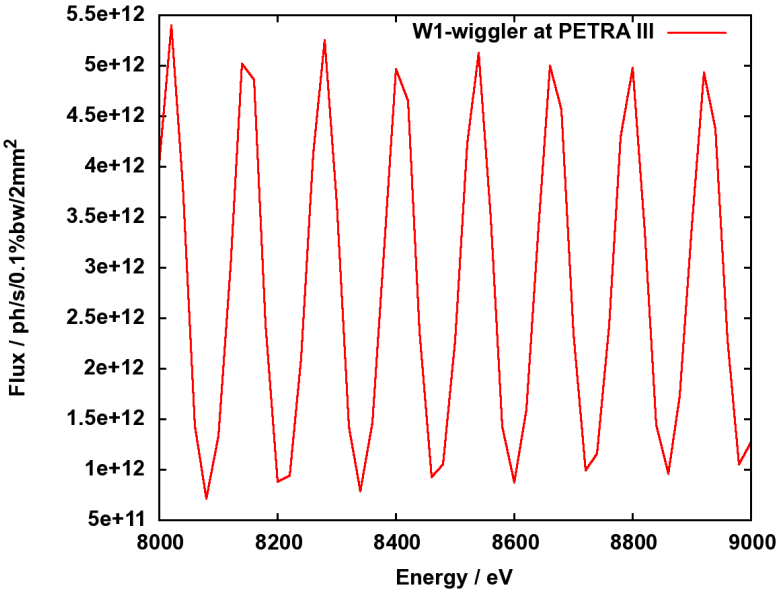

Figure 4: Flux delivered by a wiggler with parameters similar to W1 installed at PETRA III into a slit with an opening of 2 mm × 1mm (h × v) at distance of 40 m from the source.

would not differ much from an undulator, however, it would have additional disadvantages like higher heatload on front-end components and optics.

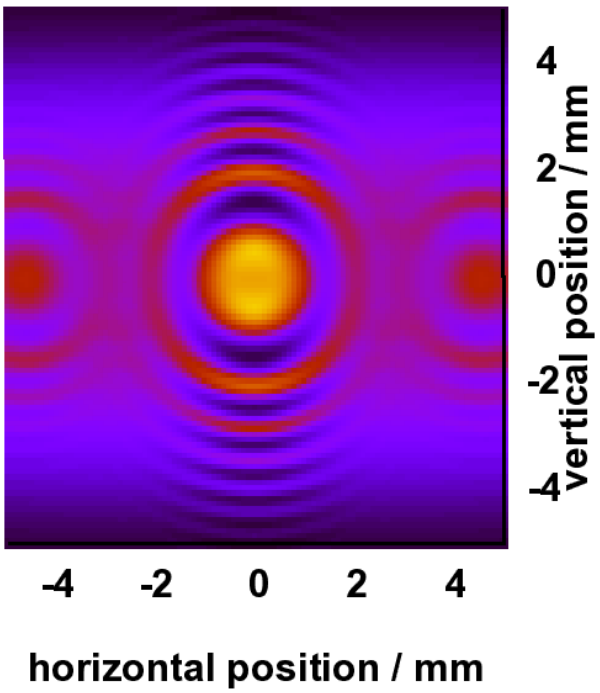

Figure 5: Intensity distribution of a wiggler at PETRA III at a distance of 40m from the source at an energy of 8020 eV. Highest intensity is yellow, lowest is black.

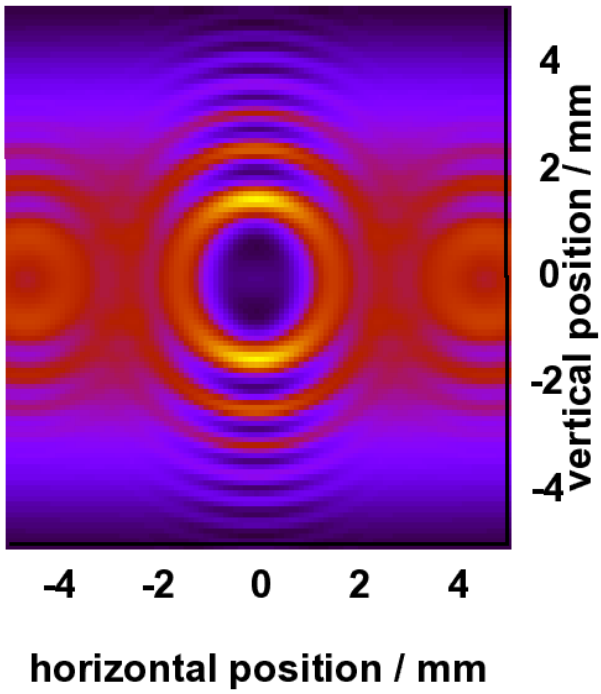

Figure 6: Intensity distribution of a wiggler at PETRA III at a distance of 40m from the source at an energy of 8080 eV. Highest intensity is yellow, lowest is black.

2.3 Undulator

Since a bending magnet or a wiggler will not work, we have to investigate how to make the best use of an undulator. In principle, we have two different modes of operation of the beamlines:

1. QEXAFS-mode with scans in the 10 ms time-scale
2. Conventional mode with scans in the 30 s - 300 s time-scale.

In the second mode of operation, the gap of the undulator has to be scanned rather slowly, which is feasible.

The existing undulators at PETRA III have a periodicity of 29 mm and 31.4 mm, respectively. The first one has a gap in the tuning curve, where the intensity is reduced by more than an order of magnitude. This is not acceptable. The second one starts on the third harmonic just below the Fe K-edge. Fe is a rather important element for catalysis research and for biology. Therefore, it is advantageous to measure Fe on the third harmonic in the QEXAFS-mode. The present energy of PETRA III is 1.4% higher than planned, i.e. 6.083 GeV instead of 6 GeV. This rather small increase, however, shifts the third harmonic too close to the Fe K-edge (see figure 8). Additionally, the minimum gap at PETRA III beamlines P06 and P09 is 9.8 mm instead of the design value of 9.5 mm, which again increases the minimum energy of the insertion device, and which results in a small gap in the tuning curve.

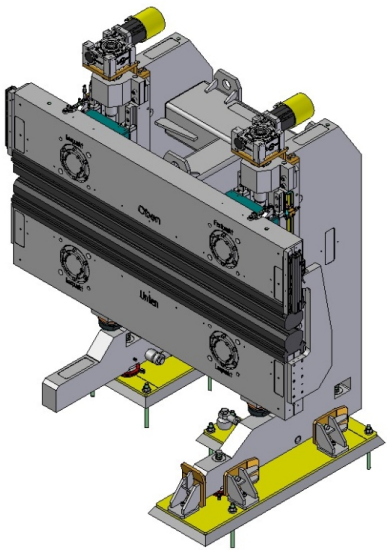

Figure 7: New design of the undulator frame for PETRA III extension beamlines. New frames were required due to the lower positron beam-height in the old octants compared to the new ones.

The following three equations can be used to find the optimum period λ_U for a given gap g and energy E: Magnetic field B_0: $B_0[T] = a \cdot \exp\left(b\frac{g}{\lambda_U} + c \cdot \left(\frac{g}{\lambda_U}\right)^2\right)$ with $a = 3.69$, $b = -5.068$, $c = 1.52$. The variables a, b, and c are material and undulator-geometry constants.

K-value: $K = 0.934 \cdot \lambda_U[cm] \cdot B_0[T]$.

Energy of the n-th harmonic: $E_n[keV] = \frac{0.95 \cdot n \cdot E[GeV]^2}{(1+K^2/2+\theta^2\gamma^2)\lambda_U[cm]}$ θ is the observation angle, and $\gamma = E/(m_e c^2)$. Since we stay on axis, $\theta = 0$.

Usually, the width of the n-th harmonic is given by $\frac{\Delta E}{E} \approx \frac{1}{nN}$ where N is the number of periods. For a tapered undulator, the width can be approximated by $\frac{\Delta E}{E} = \frac{K^2}{1+K^2/2} \cdot \frac{\Delta g}{\lambda_U} \cdot \left(b + 2c\frac{g}{\lambda_U}\right)$.

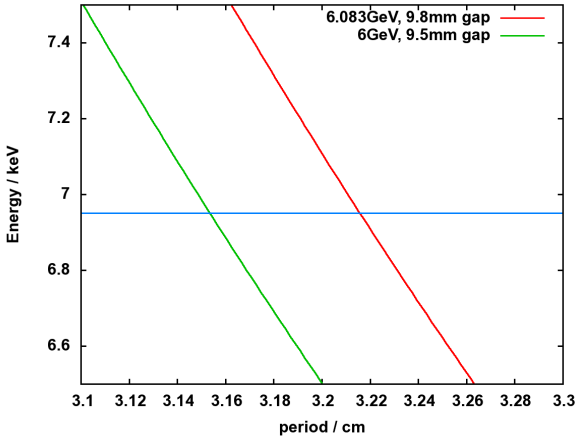

Figure 8: Energy of the 3^{rd} harmonic for different periods with the existing parameters and the design parameters at PETRA III. The blue line is the lowest energy required for Fe K-edge EXAFS scans.

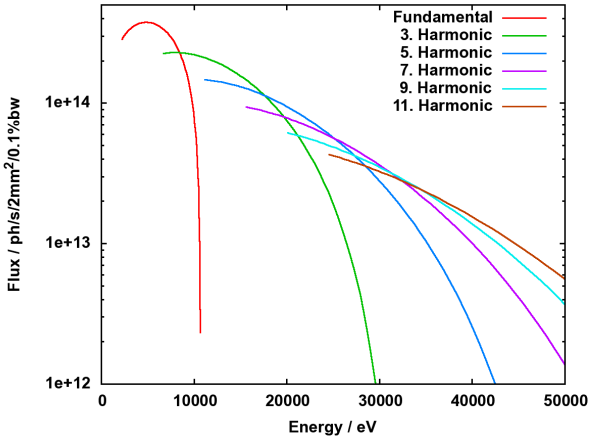

Figure 9: Tuning curve of a 2 m long U32.0 over the requested energy range. The different harmonics have reasonable overlap.

For obvious reasons, it is best to have a short period. This additional boundary condition can be used to determine the period which is required for the desired undulator properties. The energy dependence of the gap, energy and period is shown in figure 8 by two different curves. The red curve is based on the present parameters of PETRA III (6.083 GeV and 9.8 mm minimum gap), while the green curve shows the design parameters. The horizontal blue line at 6.95 keV intersects the green curve at 3.1536 cm, and the red curve at 3.2158 cm. Since we want to measure Fe QEXAFS on the third harmonic, we have to chose the parameters such that we can start the energy scan about 150 eV below the edge at 7.112 keV. Therefore, the existing U32 with a period of 3.14 cm is not suitable even with the original design values of PETRA III. If it is possible to improve the undulator chamber such that it is possible to close the gap to 9.5 mm, we can chose a period of 32.0 mm, however, if the gap

can be closed to 9.8 mm only, we have to increase the period to 32.2 mm. It is difficult to change the energy of the ring to a specific value since it is quite difficult to predict if stable operation is possible at that energy. Since we will change again the lattice of PETRA, it is to be expected that a new working point with a new energy will be found. Therefore, we assume in the following discussion that we will have a period of 32 mm. The differences in brightness and divergence are rather small for those small changes in period. The tuning-curve of such an undulator is shown in figure 9.

A typical EXAFS-scan covers an energy-range of about 1650 eV (150 eV below the edge and 1500 eV above the edge), which corresponds to a k-value of about 20 $Å^{-1}$. This translates into gap changes of 0.4 mm at higher energies at higher harmonics up to 3.75 mm for lower energies on the fundamental. The necessary speeds fall into a window of 1.5 μm/s to 125 μm/s, which is well within the specifications for the undulator, which can be moved continuously with sub-micron/s speeds.

2.3.1 Tapered Undulator

The QEXAFS-scan requires a tapered undulator since it is not possible to oscillate the gap with frequencies of 10-50 Hz. Tapering the undulator creates a gradient in the magnetic field, which results in a broadening of the undulator spectrum. At the same time, the intensity is reduced significantly. From the above equation, it is obvious that the width of the spectrum is proportional to the taper and to the harmonic. In order to cover a reasonable energy range for an EXAFS-scan, we require a taper of at least 2 mm (see figures 10 and 11).

The two undulator spectra in figure 10 have a width of about 1.55 keV, which is sufficient for a reasonable EXAFS spectrum. The flux in 0.1% bw is about 10^{13} ph/s, which translates to about 10^{12} ph/s in a monochromatic beam on the sample, which is the desired value for 100 EXAFS-scans per second with about 1000 points. At higher energies on the third harmonic, the total bandwidth increases slightly, and at higher harmonics, it is also larger than 1.5 keV for a taper of 2 mm.

The remaining problem are lower energy edges like the Mn K-edge, which cannot be measured with the third harmonic. In this case, two options are available. The first one is to use the fundamental. In that case, the bandwidth is about 1.2 keV with high flux of the order of $2.5{\cdot}10^{13}$ ph/s/0.1%bw/mm^2. A larger bandwidth with slightly reduced flux would be desirable. Another option would be the use of the second harmonic, which is already intrinsically broader. In that case, a bandwidth of 1.5 keV can be easily obtained even with a taper of less than 2 mm, however, the flux is significantly lower by a factor of about 50. Even in that case, about 50 scans with 1000 points can be measured in 1 s with 10^7 photons in the integrating time-window.

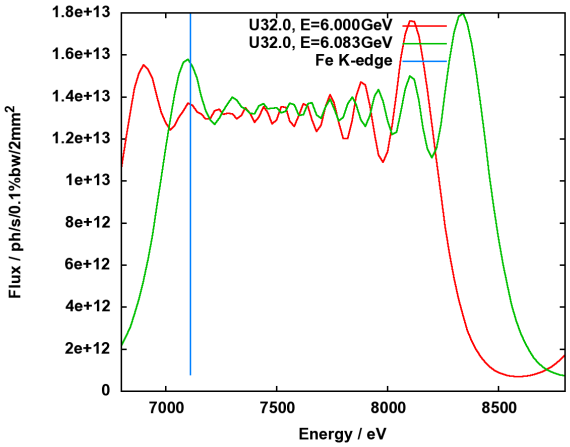

Figure 10: Effect of taper on the undulator spectrum. The two curves show the spectra of the third harmonic at a gap of 10.5 mm with a taper of ±1 mm over the entire undulator at the design and actual energy of PETRA III. The vertical line gives the energy of the Fe K-edge.

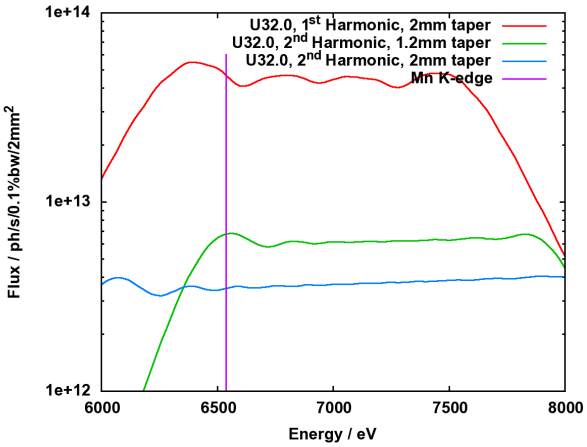

Figure 11: Spectra of a tapered undulator with the energy tuned to the Mn K-edge. The gap is tuned such that the first or the second harmonic can be used.

If it is possible to increase the taper from 2 mm to 3 mm, the fundamental can be used also for the Mn K-edge and elements with edges at lower energies.

Table 2: Energy and energy range of Mn and Fe K-edge EXAFS for different taper of the undulator, and the expected flux.

Element	Energy	Energy Range	Harmonic	Taper	Flux / ph/s/0.1%bw/2mm^2
Mn	6539 eV	1200 eV	1^{st}	2 mm	$5{\cdot}10^{13}$
Mn	6539 eV	1500 eV	2^{nd}	1.2 mm	$7{\cdot}10^{12}$
Mn	6539 eV	>2000 eV	2^{nd}	2 mm	$3.5{\cdot}10^{12}$
Fe	7111 eV	2000 eV	3^{rd}	2 mm	$1.2{\cdot}10^{13}$

2.3.2 Undulator gap scans

For an ordinary EXAFS scan over 1000 - 1500 eV it is necessary to scan the undulator gap synchronized with the scan of the DCM. For P65 this will be the only mode of operation. Both DCM and the undulator will be scanned in a continuous mode to avoid overhead of the control system and the mechanical problems caused by stepwise scans. Typical scan times will be of the order of 1 - 5 min per spectrum (1200 eV). The maximum scan speed of the undulator is high enough to enable the registration of complete EXAFS scans (1200 eV) within 1 - 2 s (see figure 12). The minimum duration of an EXAFS scan is thus not limited by the insertion device.

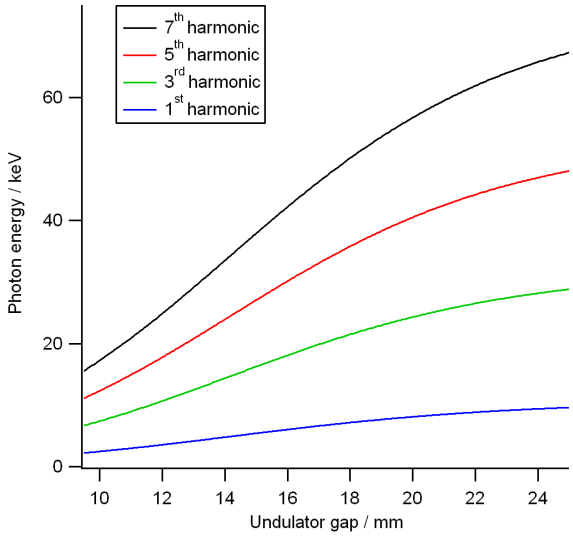

Figure 12: Dependence of the photon energy from magnetic gap

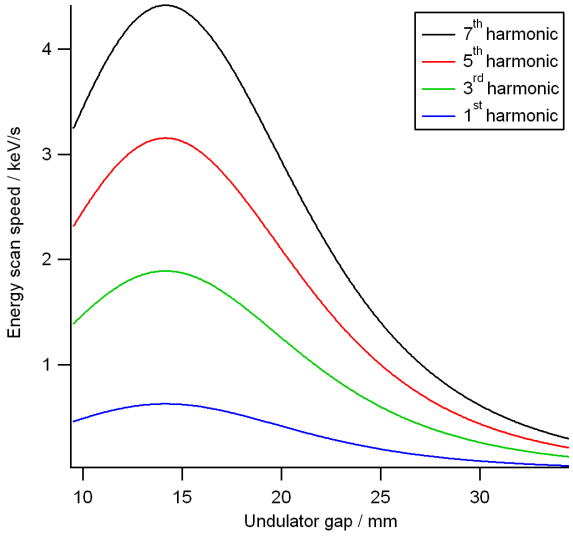

Figure 13: Maximum energy scan speed for the U32.0 undulator

The synchronisation of undulator gap and DCM scans is critical for the performance of the beamline and must be available at the first day of beamline operation. It is planned to move the undulator gap as 'slave' following the DCM encoder signal. A variable gap scan speed is already on the agenda of the undulator control system.

A first test version was successfully implemented at beamline P06 (Wellenreuther, 2012). This solution requires communication between DCM encoder and undulator controller via the TANGO software layer. The maximum deviation between the actual undulator position and the requested position was 2 eV at E = 9000 eV. This is much smaller than the FWHM of ΔE=90 eV of the undulator at this energy, and this small deviation is already better than required. The scans were also fast enough to perform 1 min per 1200 eV scans without problems.

To avoid the time consuming communication via TANGO and to make the system more stable the final solution will be implemented directly in the undulator control system which will read directly the encoder signal from the DCM. First tests of this system are scheduled for Autumn 2012.

2.3.3 Possible extension of the working range to energies between 2.4 keV and 4 keV

Some users demanded X-ray photon energies <4 keV, down to the S K-edge at 2.4 keV. With the chosen undulator parameter this is possible. K = 2.7, which is reachable with a minimum magnetic gap of 9.5 mm, corresponds to a 1st harm. Energy of 2.363 keV.

3 Beamline P64

3.1 Optical Layout of the beamline

The following requirements have to be met by the optical layout of the beamline in order to fulfil the users requirements and to make best use of the undulator.

- Energy range 4-44 keV
- Energy resolution $1.5 \cdot 10^{-4} - 5 \cdot 10^{-5}$
- High flux $> 10^{12}$ ph/s/0.014 % bw/2mm^2
- Suppression of higher harmonics, less than 0.1 % of fundamental
- Flexible beamsize 50 μm - 1 mm
- Different focal positions within the experimental hutch.

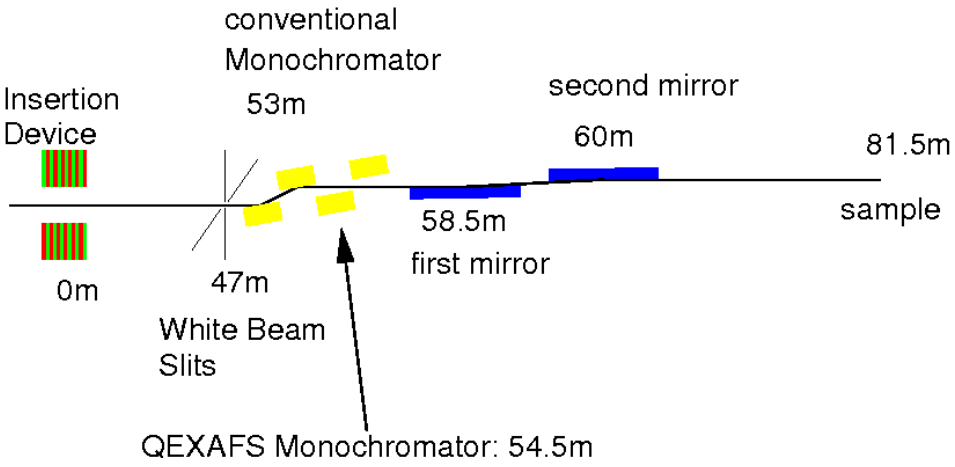

Figure 14: Optical layout of the beamline with approximate positions of main optical components. Shutters, monitors and additional slit systems are omitted in this sketch.

The design of the beamline follows the general trend of EXAFS-beamlines, which has proven a rather stable mode of operation. The first optical component is a high-heatload monochromator, which is followed by two mirrors for suppression of higher harmonics and for focusing, if desired. This arrangement is shown schematically in figure 14. The approximate positions of all optical components are given in table 3.

3.1.1 The Monochromator

The monochromator is the standard PETRA III high-heatload monochromator (see figure 15) with some modifications, which make the monochromator more stable. The most significant changes are the omission of two piezo-driven actuators for fine-adjustment of the

Table 3: Positions of various components in the beamline. The origin is the middle of the undulator. All positions are not fixed now, and can easily vary by several meters.

graphite filter 0.1 mm, 3 mm	45 m		Fluorescence screen	61.5 m
white beam slits	47 m		Photon shutter	62 m
white beam monitor	48 m		Slit system	80 m
safety shutter	49 m		Diamant window	80.5 m
monochromator	53 m		Ion chamber	81 m
QEXAFS-monochromator	54.5 m		Sample	81.5 m
Slit system	56 m			
monitor, fluorescence screen	56.5 m		Slit system	87 m
white beam stop	57 m		Monitor	87.1 m
Cylinder mirror	58.5 m		Sample	87.2 m
Bendable mirror	60 m		Spectrometer	

roll and height of the second monochromator crystal. These additional motions are not required for stable operation of the monochromator, and they might be a source of undesired beam instabilities. The requirements for repeatability and minimum step-resolution remained essentially the same.

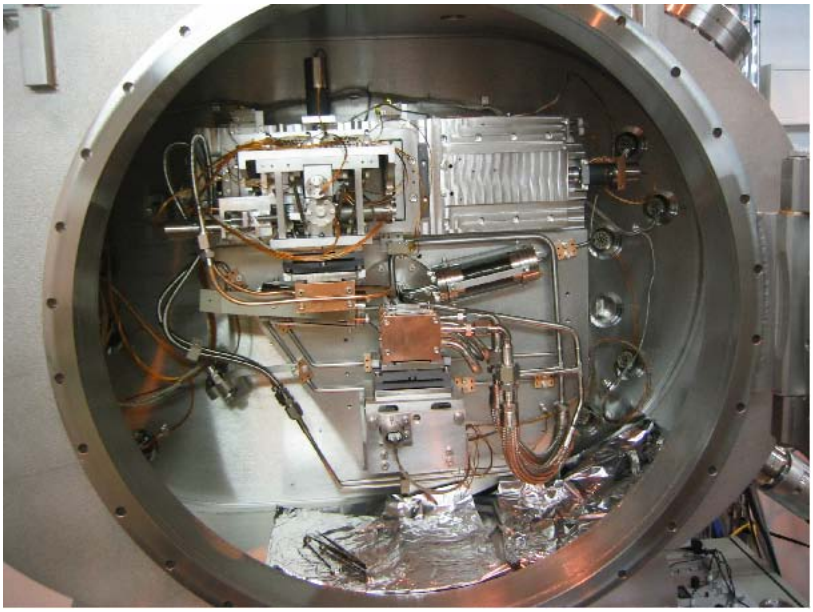

Figure 15: PETRA III high-heatload monochromator

The first crystal is mounted on a copper block, which is cooled directly with liquid nitrogen. The second crystal is cooled in a similar way with less cooling-power. The monochromator mechanics cover an angle range of $5 - 54°$, which translates into an energy range of 2.4 – 22.5 keV with the Si(111) reflection and 4.7 – 45 keV with the Si(311) reflection. The monochromator is fixed-exit with a beam offset of 21 mm. Due to the large copper cooling-

block, the surface of the first crystals stays on the rotation axis, and the second crystal is translated vertically and horizontally in order to maintain the fixed-exit condition. Both tilt and yaw of the second crystal can be tuned separately for alignment purposes, and the tilt of the second crystal can be controlled by a piezo tilt-table for feedback and detuning.

The existing monochromators at PETRA III beamlines have shown that the monochromator can cope with the heatload of even a 10 m long insertion device. Some flexures, which are not used in the existing monochromators, will be omitted for stability reasons. Two different crystals can be mounted on the cooling block, and the standard configuration with Si(111)- and Si(311)-pairs fits the requested energy range extremely well. If it becomes necessary to go to higher energies, the Si(333) or Si(444) reflections can be used.

3.1.2 Mirrors

The main purpose of the mirrors is to suppress higher harmonics, which is essential to obtain high-quality EXAFS-spectra. Therefore, different coatings and tilt-angles of the mirrors have to be combined for optimal performance. Two separate mirrors will be used in order to keep the beam horizontal. Additionally, the combination of two reflections results in a better suppression of higher harmonics, and they can be used for separate horizontal and vertical focusing.

The substrate of the mirrors is Si. Two stripes will be coated with Pt and Rh, respectively, and one stripe will remain uncoated. Furthermore, the first mirror has two different cylinders with Rh-coating and no coating for horizontal focusing. The second mirror may be bent for vertical focusing. These different coatings in combination with incident angles between 2 and 5 mrad can be used efficiently to suppress higher harmonics between 4 and 35 keV. Focused beam operations are also possible between 4 and 20 keV.

Table 4: Angle of incidence for different coatings, reflectivity within the desired energy-range, and bending radii of the cylinders for focusing for both major experimental set-ups.

E range / keV	**EXAFS**	**RXES**	**Angle / mrad**	**Reflec.**	**Coating**	**Radii / (km, cm)**	**Focus / μm^2**
4 - 9	X		3.3	>85 %	none	9.6 , 10.9	92x14
		X	2.8		none	13.2 , 10.9	120x21
7 - 20	X		3.0	>85 %	Rh	10.6 , 9.9	93x14
		X	2.6		none	14.6 , 9.9	120x21
15 - 40	X		2.0	>75%	Pt	∞	2000x700
		X	2.0		none	∞	
35 - 45				No mirror			2000x300

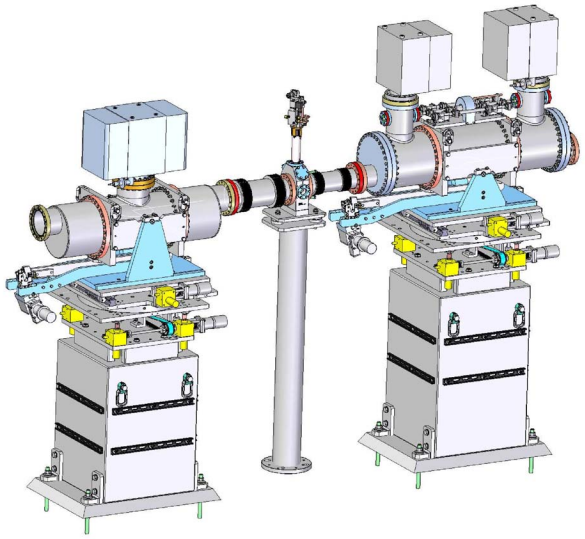

Figure 16: Design of the two mirror chambers with a fixed monitor in between them. The second mirror is bendable

The high-heatload monochromator is installed 53 m downstream of the undulator. Next, the QEXAFS-monochromator from the university of Wuppertal follows. Therefore, the closest position of the mirrors to the source is 58.5 and 60 m, respectively. The sample position for EXAFS is at 81.5 m and that for the emission spectrometer at 87.2 m. This results in a 1:2.5 and a 1:2 focusing condition, respectively. This might be reasonable for the horizontal beam size, but it might be better to work with a not optimized vertical focus, since the users prefer to study the average in the response of their sample and not the properties of one single grain. The various energy ranges, which will be covered by the different coatings on the mirrors, together with the mirror parameters and with the expected beam-size are listed in table 4.

In order to check the suppression of higher harmonics, ray-tracing calculations are performed, which include the reflectivity of the mirror (see figure 17) and of the monochromator. Additionally, the monochromator is detuned to 80 % of the maximum intensity, which is usually done with the existing monochromator feedback system. At 4 keV, this results in total transmission of 70 % through the monochromator and the mirrors, and to a total harmonic content of $9{\cdot}10^{-6}$ at 12 keV on the third harmonic of the monochromator and of the undulator. At 7 keV, the numbers are not so favourable for the Rh-mirror, since the suppression is just about 0.4 %, if the monochromator crystals are detuned by 0.012 mrad, which results in a suppression of the harmonic to 74 %. In that case, one could increase the detuning-angle slightly, which will lower the intensity of higher harmonics faster than that of the fundamental, or still work with the Si-stripe if the maximum energy does not exceed 9 keV. If the beam is not focused, it is always possible to increase the incidence angle of the mirrors, which will automatically reduce the intensity of higher harmonics. For focused beam operations, this trick will not work since the sagittal focus is directly linked to the incidence angle. In that

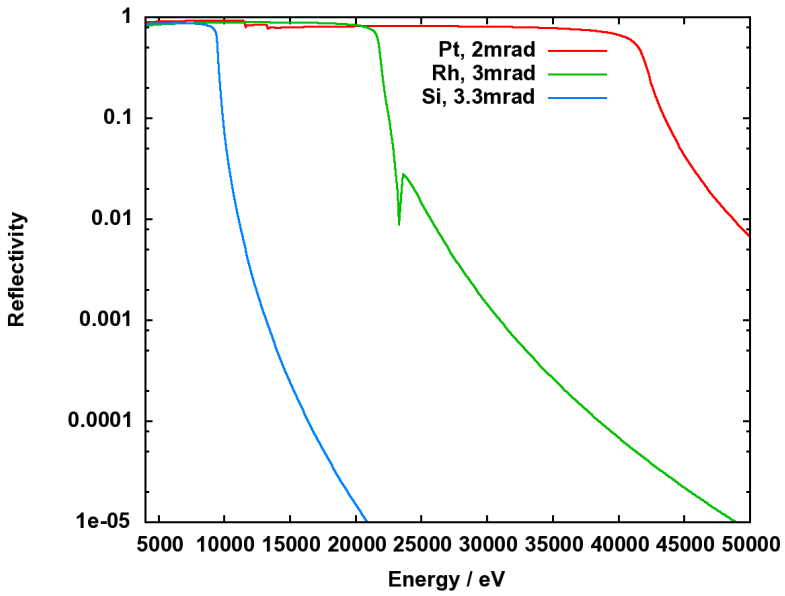

Figure 17: Reflectivity of two mirrors for various coatings and angles of incidence

mode of operation, it will be just possible to focus the beam vertically, since the meridional focus can be adjusted.

3.2 The QEXAFS Monochromator

The QEXAFS monochromator is specially designed for quick EXAFS measurements in the sub second regime. The monochromator crystals are driven in an oscillatory manner enabling a very fast and continuous scanning of the photon energy. The monochromator crystals are lN_2-cooled to cope with the heat load of the insertion device. Scan speeds of 10 ms per XANES/EXAFS-scan will be accessible in the standard operation mode.

The entire drive mechanism of the monochromator is located on the atmospheric side of the monochromator, which simplifies the general maintenance of the mechanical components and their necessary water cooling. Figure 18 shows the opened monochromator vessel on the provisional support frame which will be used for initial tests.

3.2.1 Monochromator crystals

The crystal stage includes two channel cut crystals (Si(111) and Si(311) cuts) mounted side by side, and the liquid nitrogen cooler. Both crystals are indirectly lN_2-cooled by laterally clamped copper cooling elements shown in figure 19. The channel cut crystals are manufactured with a gap of 12 mm resulting in a beam offset larger than 20 mm, which is the minimum required at PETRA III due to radiation protection. With both crystals photon energies between 4 keV and 36 keV will be accessible (table 5). Crystal changes are

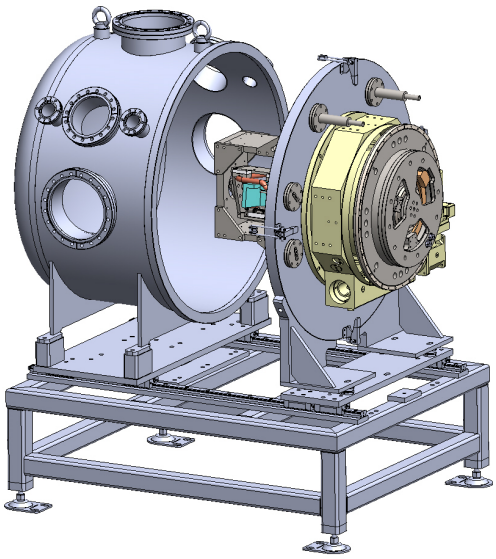

Figure 18: Drawing of the QEXAFS monochromator. The monchromator vessel is mounted on two rails which allow a lateral movement and comfortable opening for maintenance purpose. Here the monochromator is mounted on a provisional support frame.

performed by remote controlled lateral movement of the entire monochromator. It will take only a few minutes to change between both crystals.

Table 5: Energy range of the QEXAFS monochromator. The monochromator will be equipped with Si(111) and Si(311) channel cut crystals, the Si(511) orientation is included as future option.

	Si(111)	Si(311)	Si(511)	Beamoffset
Θ/deg	E / keV	E / keV	E / keV	δs / mm
6	18.914	36.217	56.742	23.9
30	3.954	7.572	11.862	20.8

Due to the channel cut design of the crystals - which is selected to obtain the best stability possible - the monochromatic beam is not at a fixed exit height and therefore the beam offset will change during the measurements. For typical scan ranges used in EXAFS and XANES measurements the height change is shown in figure 20. As can be seen the vertical beam offset is always smaller than 0.1 mm in the case of XANES scans and thus serious problems due to the vertical beam movement during an energy scan are not expected. This statement is backed by the experience with experiments at existing QEXAFS-monochromators with similar crystal gap sizes.

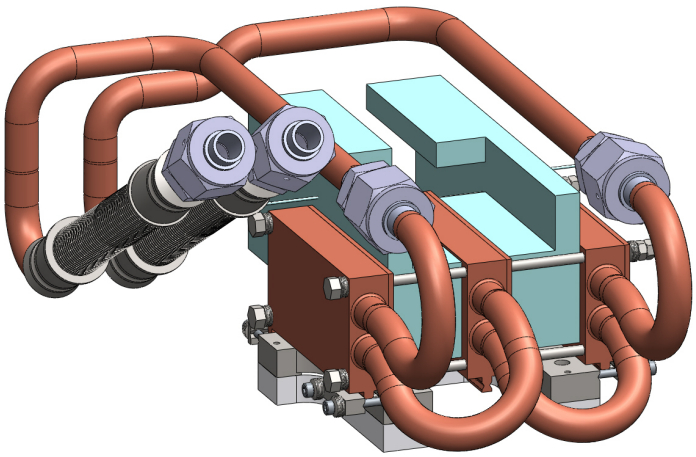

Figure 19: The crystal stage showing the two crystals, the liquid nitrogen cooler and their support structure.

3.2.2 The Drive Mechanism

A direct drive mounted on a large goniometer on the atmospheric side of the monochromator is used to oscillate the Bragg axis. This movement is coupled to the crystal stage and into the vacuum by means of a ferrofluidic sealed rotary feedthrough. The central Bragg angle and thus the photon energy is determined by an optical encoder (Renishaw Tonic) attached to the goniometer. The oscillatory movement is tracked by an optical encoder of the same type which is mounted inside the motor. This set-up will allow detecting and correction of deviations of the angular position at the goniometer due to load alternation at the returning points of the oscillation movement. Both encoders are at the atmospheric side and thus are easily accessible for service, e.g. if a replacement becomes necessary due to possible radiation damage. At a later stage another angular encoder might be added directly to the crystal cage, yielding the sum of both angles directly.

The achievable oscillation frequency depends on the required amplitude and is mainly limited by the mass moment of inertia of the moving parts, in particular the crystal stage and the motor itself. The calculated usable amplitude as a function of the oscillation frequency is shown in figure 21. The operation of the monochromator within the shaded area will be possible under remote control. This area can be extended in future by reducing the mass moment of inertia, which for instance can be achieved by choosing light metals such as titanium instead of steel for the construction of the crystal stage and the motor.

Two different operation modes will be implemented. For frequencies of up to 50 Hz the motor can be driven in a closed loop environment. This mode will not only allow to perform the classical sinusoidal oscillations of the Bragg axis, but also to program arbi-

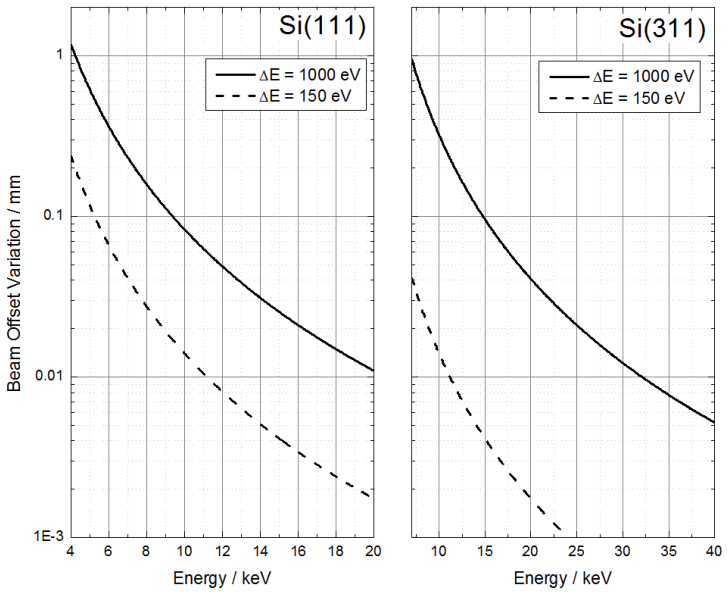

Figure 20: Vertical variation of the beam offset during typical XANES ($\Delta E = 150\,eV$) and EXAFS ($\Delta E = 1000\,eV$) measurements as function of the start energy of the scan.

trary trajectories. This feature will be most promising at low frequencies around 10 Hz, i.e. 50 ms/spectrum, and can be used to improve data quality by specifically reducing the scan speed at higher k values. Closed loop operation at higher frequencies is currently limited by the time constant (2 ms) of the embedded PID controller.

In order to use higher frequencies of up to 100 Hz the motor will therefore be used open loop. The trajectory in this mode is restricted to a sinusoidal oscillation. It should be pointed out that the usable amplitude at 100 Hz still amounts to 0.5°, which is large enough for XANES measurements at all accessible absorption edges (figure 22). So very fast quick XANES measurements of up to 200 spectra per second - resulting in a time resolution of merely 5 ms - becomes feasible. The high intensity of the undulator source in such a small bandwidth will allow excellent signal to noise ratio, also in the case of fluorescence detection.

However, it has to be mentioned that the extreme intensity of PETRA III already created some problems with radiation damage at existing monochromators in encoders and piezo-actuators. Those experiences are continuously included in the design of the QEXAFS-monochromator, but new effects might show up which have to be dealt with in an iterative manner to obtain the best performance.

The QEXAFS monochromator described in this section will have - considering existing and planned beamlines worldwide - an outstanding performance and explore the current limits of the technique.

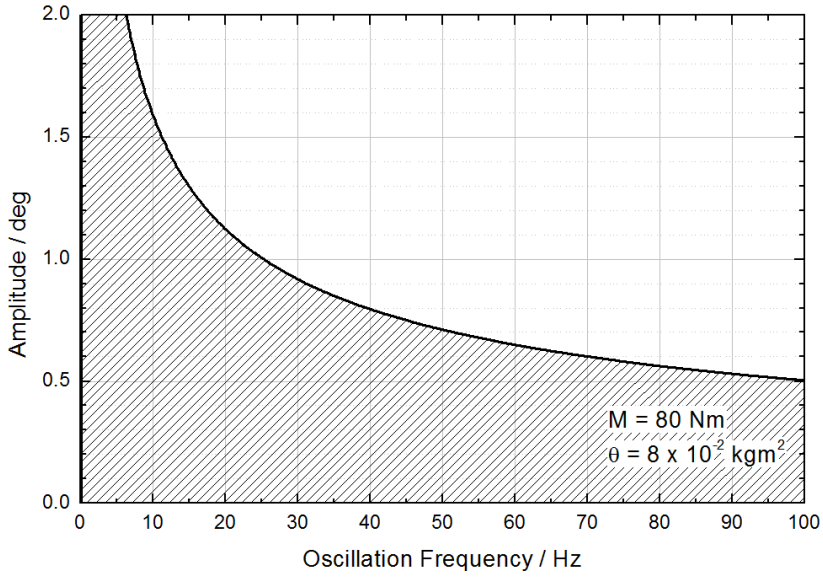

Figure 21: Operation range of the QEXAFS monochromator using the indicated torque M and the mass moment of inertia θ.

3.3 End-Station

In principle, the set-up of the end-station of P64 will be a combination of DORIS III beamlines C and W1. A preliminary sketch is shown in figure 23. A standard EXAFS set-up with three ion-chambers for measurements in transmission geometry will be mounted in the up-stream part of the hutch. Additionally, several types of detectors will be used for fluorescence-mode experiments. Some experiments can be still done with total fluorescence-yield detectors like a PIPS-detector (large Si-diode for lower energies up to 12 keV) and a Lytle-detector (large area ion-chamber for higher energies above 12keV), others require an energy-dispersive detector like a Ge solid-state detector with an energy resolution of better than 200 eV and photon count rates of more than 10^6 Hz. A few PIPS-detectors are already available at the existing DORIS III EXAFS beamlines. Furthermore, one Lytle-detector is also available, however, it might be a good idea to improve the electronics of that detector for safe operation and reduced noise.

A 100-element Ge-detector for P64 has already been purchased by DESY within the BMBF funded project in collaboration with the University of Paderborn. The detector is almost finished and the factory acceptance test will is planned within the next few weeks. Special program codes for speed-optimized use of the detector with modern VME hardware are part of the BMBF-project.

We are still discussing if we should also install bent-Laue crystal analysers with a large bandwidth. These analysers have a better energy resolution than a Ge-detector, and they might find some applications in pathological cases like Eu in Fe or similar.

Finally, a high-resolution spectrometer for emission spectroscopy will be installed in the

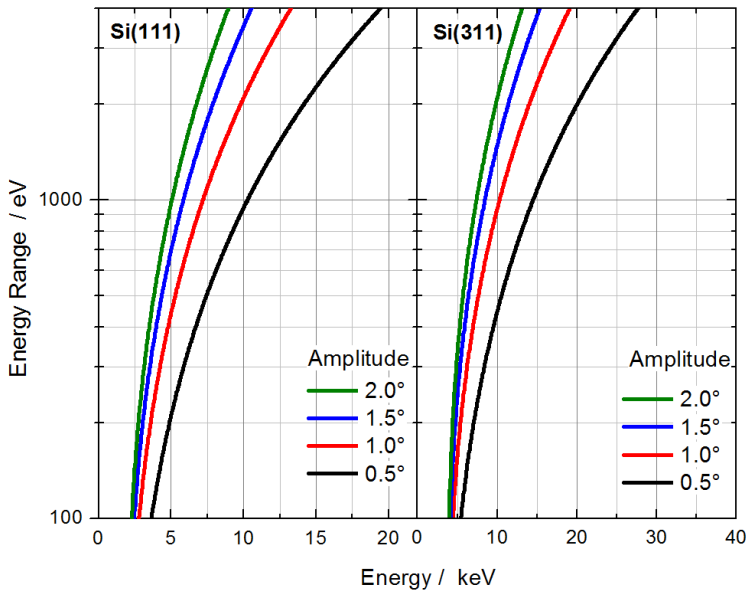

Figure 22: Usable energy range for XAS measurements in dependence of the oscillation amplitude as a function of the initial photon energy.

down-stream part of the hutch. Such a spectrometer is being operated at DORIS III at beamline W1, and several user groups want to extend their use of this spectrometer with the expected higher flux and better energy resolution at P64. Optionally, the spectrometer can be upgraded from a single-element analyser to a multi-element analyser system in order to increase the signal by another order of magnitude. Several user groups have shown interest to submit a proposal for additional BMBF-funding.

3.4 Sample Environment

Since EXAFS is applied in a large variety of scientific fields, different sample environments are required. Some experiments are performed at low temperatures. For those experiments, a liquid He-flow cryostat is the best choice. One such cryostat is already available for the existing EXAFS beamlines at DORIS III, so it will increase the flexibility of the beamlines if a second one will be purchased. Additionally, a closed-cycle cryostat is also being purchased with funds from the BMBF Verbundforschungsprojekt.

EXAFS also finds many applications at high temperatures. For that purpose, a standard oven like a LINKAM stage for temperatures up to 1500°C with heating and cooling rates of 200°C/min are quite well suited. However, the majority of users from catalysis research prefer to use their own stages for heating and cooling cycles.

Some samples are just thin films on a substrate. In order to optimize the signal, a grazing-incidence geometry with a small tilt-table with high precision is required. Due to

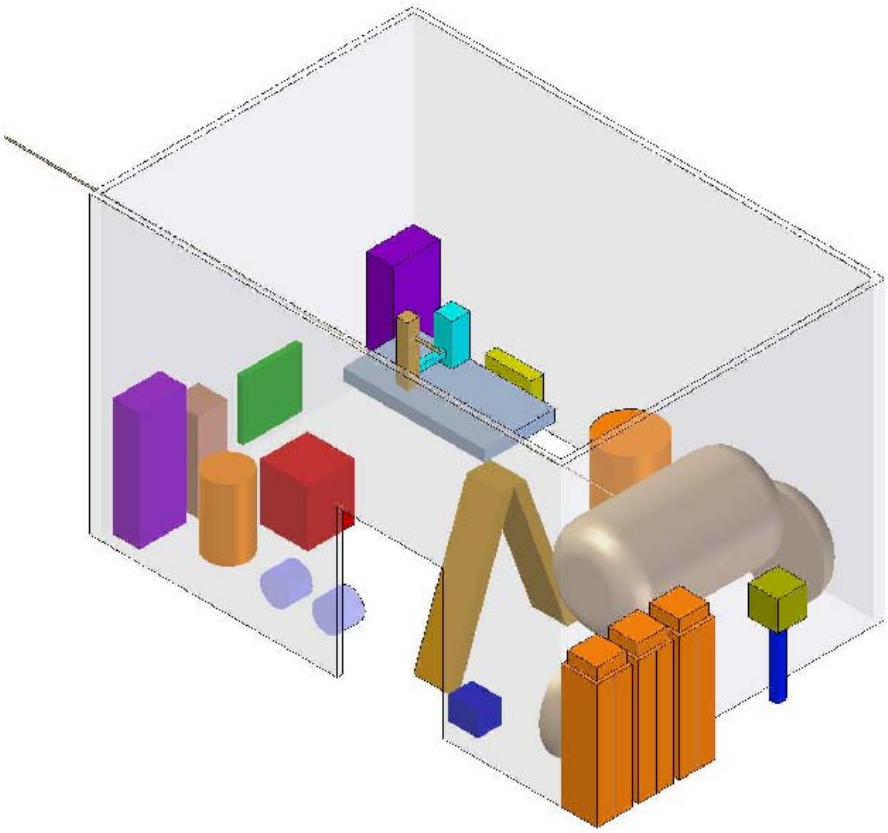

Figure 23: Layout of the experimental hutch of P64 with the standard EXAFS set-up in the upstream half, and the emission spectrometer from W1 in the downstream half. Some additional equipment (dewars, pumps, etc.) are also installed.

the small beamsize of a focused beam, and the lower divergence at P64 compared to the existing DORIS III beamlines, a new tilt-table might be required. If possible, the crossed arcs from W1 will be transferred to P64.

One major application of P64 will be in-operando catalysis research. These experiments require the use of several toxic, flammable or other hazardous or harmless gases. Additionally, new samples have to be prepared with these gases while others are still being measured in order to optimize the utilization of beamtime. Therefore, several gas-lines will have to be installed in the experimental hutch.

4 Beamline P65

4.1 General beamline layout

The design of P65 is determined by several boundary conditions. First and most important are the demands of the potential user community. Table 6 gives an overview about their demands. The listed requirements are the condensed summary of 2 user workshops held in 2010 and 2011. The second important boundary condition is the need to re-use several key beamline components like monochromators from existing DORIS III bending magnet beamlines. This imposes limits for instance on the maximum tolerable power load on the optical components. The third boundary condition are the storage ring properties, namely the small emittance at high electron energy and the large radius that requires large distances between the source and the first optical elements (Franz et al., 2006). The proposed design considers all these boundary conditions.

Table 6: Key parameter of beamline P65

Beamline parameter	**User demand**
Energy range	Cover the K or L3 edges of all relevant elements
Integral photon flux (10^{-4} BW)	$> 10^{10}\mathrm{s}^{-1}$
Beamsize	Millimetre range
Scan time	1 - 5 min per scan
Experimental hutch	• Large enough for in-situ equipment • Infrastructure for use of gases and other media like pressurised air and cooling water • Liquid He and N_2 Cryostats

Taking into account the PETRA III machine properties the above mentioned user demands are best fulfilled using the following straightforward design:

Experiments at P65 will use the radiation produced by a short 12 period undulator. A water cooled fixed exit double crystal monochromator (DCM) will be installed at a distance of ca. 50 m from the source. Two plane mirrors will be used to cut off higher harmonics radiation. The first mirror will be water-cooled and absorb a significant part of the power emitted by the undulator. This way the power load on the 1st DCM crystal can be reduced to tolerable values. To cover the energy range between 4 and 44 keV the plane mirrors will

be covered with different materials and must be usable at variable angles of incidence. For the highest energies a minimum angle of incidence of 1.5 mrad is foreseen.

The experimental hutch provides enough space for all kinds of experiments, even with the large experimental set-ups usually needed for in-situ experiments. A sufficient number of gas lines, exhausts, sensors etc. will make it possible to work with problematic gases like H_2S, NO_x, CO, H_2 etc. at the beamline. Similar to the X1 Beamline at DORIS III a chemistry laboratory adjacent to the experimental hutch will allow the users of beamline P65 and P64 to prepare and condition their samples and to measure them without delay. Figure 24 gives a schematic overview of the beamline. Details of the set-up will be discussed in the following sections.

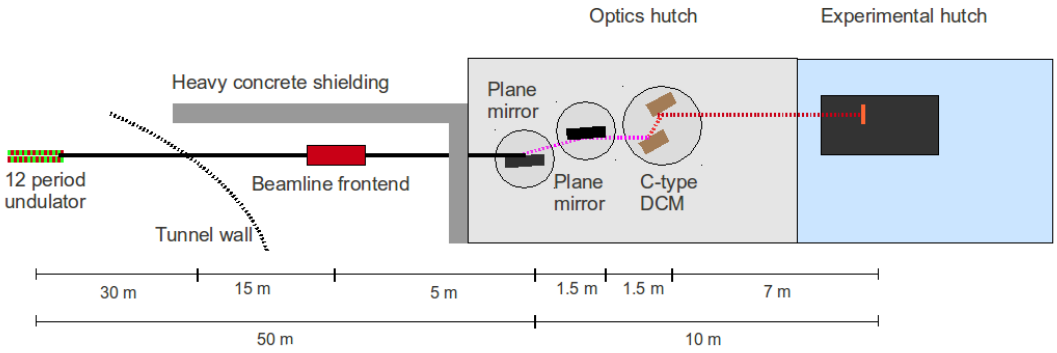

Figure 24: Schematic drawing of beamline P65, all dimensions are approximate

4.2 X-ray optics

4.2.1 Double crystal monochromator

The new beamline will be equipped with one of the established and well-performing water-cooled fixed-exit DCM (see figure 25) that are today used for EXAFS spectroscopy at beamlines C and A1 (C-type DCM). Two crystal pairs, a Si(111) and a Si(311), will be installed in the DCM to cover the energy range between 2.4 and 44 keV (Rickers et al. 2007, Welter, 2010).

The beamline design will reserve enough space to replace the C-type DCM with a cryogenically cooled high power load DCM at a later date. This option will however only be used if it turns out to be impossible to use a 12 period undulator and if a significantly shorter undulator (like 5 periods) must be used to reduce the power load of the first crystal.

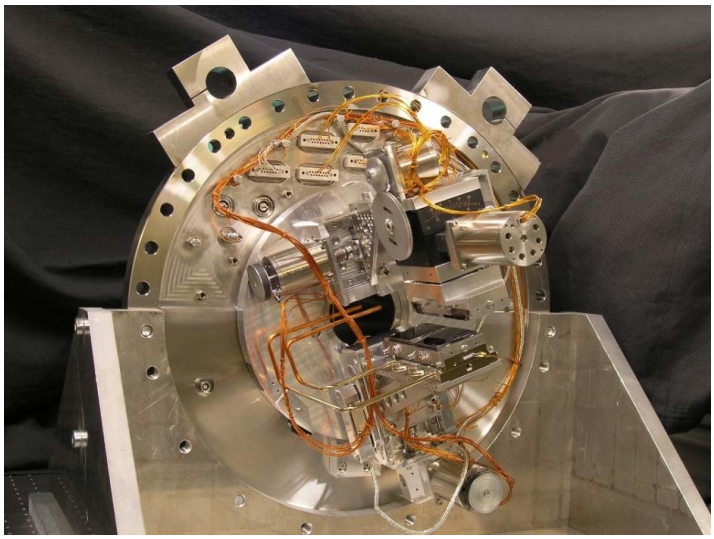

Figure 25: C-type DCM without vacuum tank

4.2.2 Power load issues

Table 7 gives an overview about the relevant parameter of the DCM. The maximum allowed power load has to be considered in the design of the source (see there). At DORIS III beamline A1 the maximum power density at an incidence angle of 90° is 0.7 W / mm^2 (see figure 26). The integral power load of the first crystal calculated for a typical beam size of $30 \cdot 1$ mm^2 is 21 W.

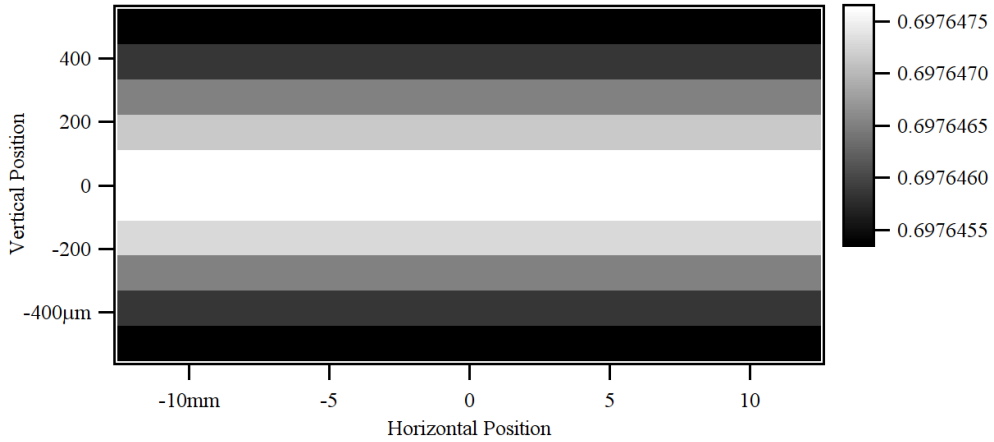

Figure 26: Power load density (W/mm^2) on the first crystal of the current A1 monochromator. Beamsize 30·1 mm^2, storage ring current and energy 140 mA and 4.45 GeV, respectively. The resulting integral power load is 21 W

Under these conditions the C-type DCM shows a good (better than 0.1 eV) reproducibility of the energy scale and even after the significant change of the storage ring current after an injection, absolutely no influence of the changing power load on the rocking curve position or width is detectable (see figure 27) (Welter, 2010) .

Table 7: Properties of the C-type DCM

DCM type	Fixed exit, 20 - 21 mm offset
DCM crystals	2 pairs, Si(111) and Si(311), $40 \cdot 40$ mm^2
DCM cooling	Water
Maximum integral power load	30 W
Maximum power load density (normal incidence)	2 W/mm^2

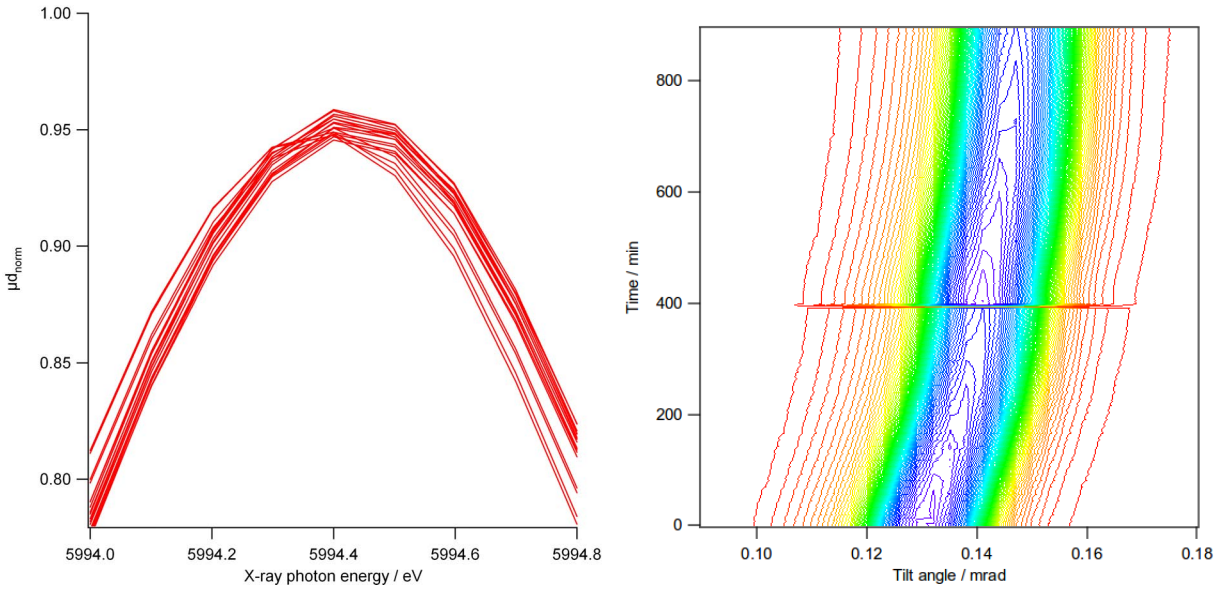

Figure 27: Left, stability of Energy of the A1 DCM, measured over one injection cycle, reproducibility of the position of the Cr VI pre-edge peak. Right, stability of rocking curve position measured over one DORIS injection. Note that the apparent broadening of the rocking curve is an artefact caused by the higher intensity after the injection (at 400 min).

4.2.3 Continuous scan mode

At P65 the DCM will be scanned in continuous mode to enable the synchronised tuning of the undulator gap. Table 8 gives an overview about the maximum and minimum scan speed of the three motors involved. t_{max} and t_{min} are the maximum and minimum scan times respectively as they are calculated from the maximum and minimum speed of the θ axis rotation. As can be seen from the values in table 9 the minimum time is always below 1 min and the maximum time is always above 5 min. At shallow Bragg angles the vertical movement of the 1st crystal is very short, just some μm. In that case the current

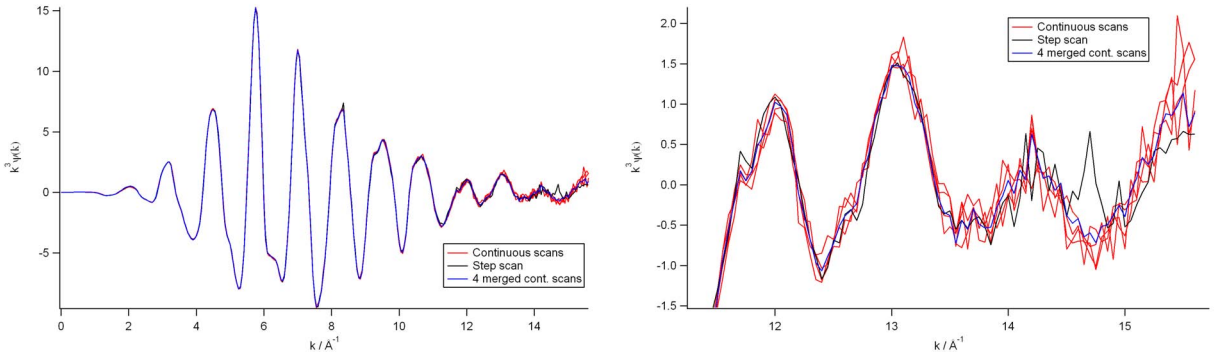

Figure 28: Left, EXAFS spectra of a Ti-foil, measured step by step (black, overall scan time 1800 s), 4 continuous scans (red, 400 s each) and merger of the 4 continuous scans (blue, Overall scan time $4 \cdot 400$ s) Right, expanded plot of the higher k region.

minimum velocity (20 microsteps / s) can only be reached with scan times below 60 s. For most applications this will be too short. Considering the minimum speed of the linear stage a 60 s scan currently requires a minimum distance of 15 μm, a 5 min long scan 75 μm.

With the ZMX motor controllers, used at PETRA III, it is however possible to divide 1 full step of the stepper motor into 512 microsteps. This is more than enough to perform 5 min long scans in the entire foreseen energy range. Alternatively at small Bragg angles the EXAFS scan might be performed without changing the height of the 1st crystal at all. The small resulting vertical movement (some μm) of the beam is irrelevant if just in front of the sample the final beam size is determined by an aperture that is some 10 μm smaller than the incoming beam.

The third movement that is necessary to change the DCM energy is the longitudinal movement of the 2nd crystal parallel to its surface. It will not be used during a continuous scan. This movement is necessary to compensate the longitudinal offset of the beam at shallower Bragg angles. The monochromator control software will optimise the longitudinal position of the 2nd crystal before a scan is started, so that no part of the beam will miss the 2nd crystal during the EXAFS scan.

Results from experiments at beamline A1 at DORIS III when the performance of the DCM during continuous scans was tested and compared with stepwise scans of the same sample are presented in figure 28. It shows a comparison between EXAFS spectra of a Ti-foil measured in continuous mode and in conventional stepwise scan mode. The stepwise scan was measured within a total scan time of 30 min. Each of the continuous scans was measured in one single 400 s long sweep with a energy spacing of 0.5 eV. All 4 continuous scans together demanded a scan time of 1600 s, very similar to the total scan time for the one stepwise scan.

Table 8: Current maximum and minimum scan speed of DCM motors during continuous scans, using 20 μsteps per fullstep and a base rate of 20 μsteps s^{-1}.

Motor	$\mathbf{V_{max}}$/ **steps/s**	$\mathbf{V_{max}}$	$\mathbf{V_{min}}$/ **steps/s**	$\mathbf{V_{min}}$
Bragg axis	15000	$0.1875°s^{-1}$	20	$2.5 \cdot 10^{-4}°s^{-1}$
1^{st} crystal vert.	15000	0.1875 mm s^{-1}	20	$2.5 \cdot 10^{-4}$ mm s^{-1}
2^{nd} crystal hor	15000	0.18757.5 mm s^{-1}	20	0.01 mm s^{-1}

The advantage of the continuous scan mode is that the integral scan time is (almost) equal to the effective scan time, because of the missing overhead caused by the DCM movements and wait times. It is clearly visible, that the spectrum with the least noise is the merged spectrum of the 4 continuous scans. This proves that the continuous scan mode makes a much more effective use of the photon beam and that, even under the conditions at a DORIS III beamline, it does not visibly suffer from beam instabilities.

Table 9: Maximum and minimum scan times of continuous scans of the DCM, resulting from the values for the Bragg-axis in table 8

Crystal	**Scan range / keV**	$\mathbf{t_{max}}$/s	$\mathbf{t_{min}}$/s
Si 111	4 - 5	25300	34
Si 111	15 - 16	1900	3
Si 311	10 - 11	8460	12
Si 311	43 - 44	461	1

4.2.4 Mirrors

Considering first the user demand for an EXAFS-beamline having a beamsize in the mm range and second the relative positions of the source, the experimental hutch and of the optics hutch, which would only allow a significant de-magnification of the beam if a focusing mirror was used, it seems advisable to use only plane mirrors.

These mirrors have two main tasks, to suppress higher harmonics radiation and to reduce the power load on the first DCM crystal. The most effective higher harmonics suppression over a large working range requires the combination of variable angles of incidence on the

mirrors and different mirror coatings. P65 is designed for the energy range (2.4) 4 - 44 keV. The range between 2.4 and 4 keV is not foreseen for day 1 operation, but should be considered in the beamline design. With a minimum angle of incidence of 1.5 mrad and a maximum angle of incidence of 4.5 mrad the mirrors can be used over the entire working range of the beamline. This is shown in figure 29 showing the reflectivity curves for Si, Rh and Pt covered plane mirrors with a conservatively estimated roughness of 5 Å under varying incidence angles.

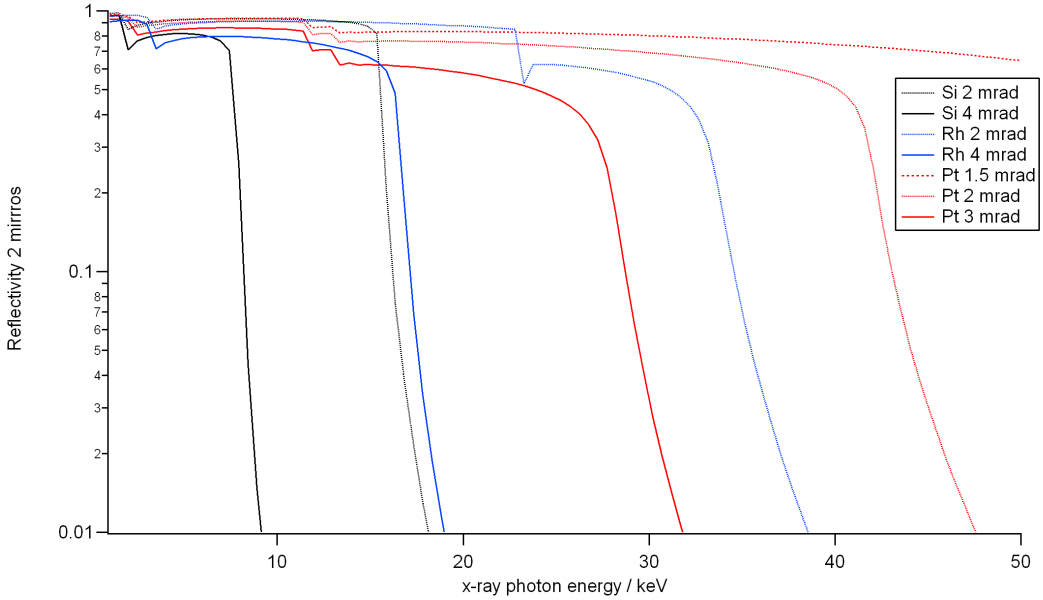

Figure 29: Cumulated reflectivity of two plane mirrors at varying angles of incidence. The presented reflectivities include the effect of a conservatively estimated value of 5 Å for the roughness of the mirror surface

Each individual stripe on the mirror can be relatively narrow; the usable horizontal width of the incoming beam is of the order of 2 mm, therefore stripes with a width of 10 mm are much more than sufficient (see source properties). For 3 parallel stripes with different coatings this results in a 30 mm wide mirror. The length of the mirror is determined by the vertical beamsize and the incidence angle. A mirror length of 1000 mm is sufficient for a vertical beamsize of 1 mm and a minimum angle of 1.5 mrad.

The final beamline design must consider the changing height of the monochromatic beam due to the varying angle of incidence on the mirrors. The distance between the two plane mirrors should be as short as possible to minimise the beam height offset caused by the mirrors. The 2nd mirror will also be placed in front of the DCM. This avoids changing angles of the incoming beam on the first DCM crystal. This set-up will, however, only be chosen if the power load on the 2nd mirror is small enough to use an uncooled mirror design. The total power load of the undulator is approximately 10 W on the first mirror. First, preliminary calculations (see figure 31) indicate that the temperature of an uncooled second mirror increases by less than 0.2 K if a total of 5 W in a rectangular beamsize of 2 x

1 mm^2 is absorbed by the mirror under an angle of incidence of 3.5 mrad. These values are rather extreme and present an upper limit of the temperature increase of the second mirror. Different finite element calculations for a water-cooled mirror in P02, which is hit by the beam from a 2 m-long undulator and sees a heat-load of 50 W, show that the flat mirror will be bent by gravitation and the heatload to a radius of 35.6 km (see figure 30). Therefore, we do not plan to cool also the second mirror.

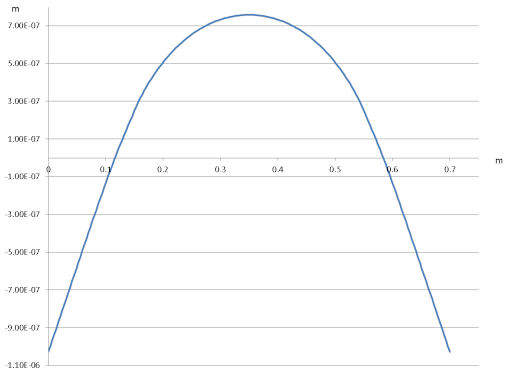

Figure 30: Results of finite element calculations for the P02-mirror, which sees about 50 W on a footprint of 2 x 400 mm^2. The blue curve shows the reflecting surface of the mirror. The mirror-mount is water-cooled. Heat-load and gravitation result in a bending of the mirror of 76 μm, which corresponds to a radius of 35.6 km.

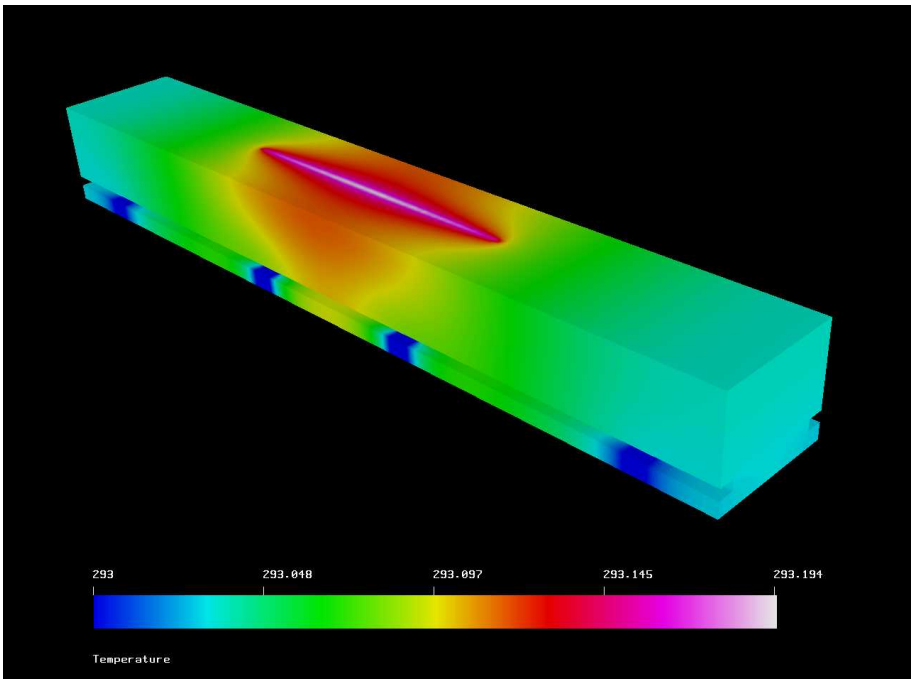

Figure 31: Preliminary results of FEM calculations to determine the temperature increase of the second mirror, if it absorbs a total power of 5 W in a beam of 2 x 1 mm^2. These values are ten times higher than the worst-case scenario.

Since all reflecting surfaces, mirrors and crystals are plane the arrangement of DCM and 2nd mirror has no influence on the beam geometry or on the flux on the sample. All calculations presented in the following sections were made for the set-up with only one mirror in front of the DCM and are therefore representing the worst case scenario for the 1st DCM crystal.

If the DCM has to be placed between the two mirrors the DCM control software must account for the incidence angle of the first mirror and correct the Bragg angle accordingly. The height of the experimental table in the hutch and of the diamond window that terminates the beamline will in either case be adjustable to follow the exit height changes caused by varying angles of incidence on the mirrors. A vacuum tube diameter of 63 mm behind the 2nd mirror chambers is sufficient if the distance between the 2 mirrors is not larger than 5 m (30 mm height difference between 1.5 mrad and 4.5 mrad).

4.3 Source

The technical and user demands on a synchrotron radiation source for P65 are listed in table 10. At a high energy low emittance storage ring like PETRA III and bearing in mind the properties of the DCM the requirements are best fulfilled by a relatively short undulator. Undulators as source for an EXAFS beamline require gap scans synchronous to the DCM scan.

Table 10: Technical and user demands on the source for P65

Parameter	
Beam size at sample position	Millimetre range
Energy range	4 - 44 keV
Overlap 1st and 3rd harmonic	At least 1500 eV
Monochromatic photon flux	$\geq 10^{10}$ s^{-1}
Scan speed	10 - 300 s for 1.2 keV
Spatial homogeneity	High, no changes during scan
Max integral power load (front end)	1000 W
Max power load density on DCM	2 W/mm^2 (normal incidence)
Front end aperture size	$6 \cdot 10$ mm^2 (v*h)

The parameters of the undulator, namely the number of periods and the maximum

electron deflection parameter K are chosen so that the power load on the first DCM crystal is below the limit of 2 W/mm^2 and that the overlap between 1st and 3rd harmonic is large enough for EXAFS scans. Table 11 shows values for the power load on the first crystal of the DCM produced by a 12 period undulator with a period length of 32.0 mm and a maximum K of 2.6. The maximum K of 2.6 corresponds to a minimum magnetic gap of 10.05 mm, the mechanical limit is 9.5 mm, this leaves a reasonable margin to compensate degradation of the magnets during operation.

In this scenario the DCM is placed behind a cooled mirror. This mirror acts as low pass filter and reduces the power load on the 1st crystal significantly. Without a cooled mirror in-front of the DCM the maximum number of periods would be 5, the resulting photon flux a factor of 4-5 smaller. At energies above 20 keV, working with the 7th or 9th undulator harmonic, the mirror will be used in combination with a cooled absorber with variable thickness (0.5 - 2 mm C or equivalent) to form a bandpass filter that further reduces the power load by filtering out the lower harmonics. This absorber will be placed in front of the mirror to reduce the power load of the mirror. The calculated values show that under these conditions the 2 W/mm^2 limit of the C-type DCM is not exceeded.

The lower energy limit of 4 keV corresponds to a K of 1.867. However, the necessary overlap between 1st and 3rd harmonic can only be achieved at a K of 2.6. So, the undulator is designed to reach a maximum K of 2.6 if the 3rd harmonic is used at energies around 7500 eV.

Table 11: Power load on the first crystal of the C-type DCM in 50 m distance from a 12 period U 32 undulator. A plane mirror with variable angle of incidence acts as low pass filter, at higher X-ray photon energies it is combined with a cooled filter to form a bandpass filter. The calculated flux into 10^{-3} bandwidth includes the losses due to the mirror and filter

E / eV	**K**	**Harm.**	**Mirror**	**Filter**	**Power load / W/mm^2**	**Flux / 10^{12} mm^{-2} s^{-1}**
4000	1.867	1	Si 4mrad	——	**0.56**	9.5
7516	2.600	3	Rh 4mrad	——	**1.22**	8.9
15000	2.306	3	Rh 4mrad	——	**1.27**	6.8
20000	2.384	7	Pt 3mrad	C 0.5 mm	**1.53**	4.4
30000	1.767	7	Pt 2mrad	C 2 mm	**1.63**	2.3
44000	1.578	9	Pt 1.8 mrad	C 2 mm	**1.54**	0.62
44000	1.867	11	Pt 1.8 mrad	C 2 mm	**1.87**	0.85

This is illustrated in figure 32 which presents a plot of the expected brilliance of the 12

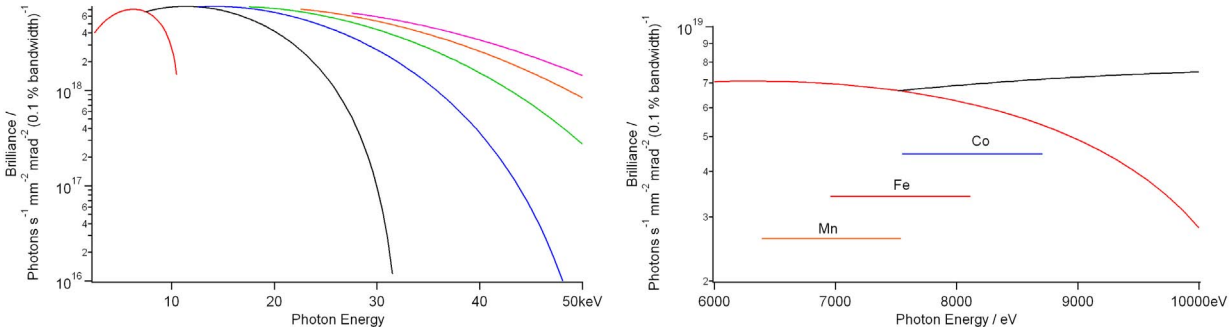

Figure 32: Left, brilliance of an 12 period U32.0 undulator with maximum K = 2.6 (magnetic gap 10.05 mm), right, overlap between 1st and 3rd harmonic and usual scan range of Mn, Fe and Co EXAFS scans.

period K_{max}=2.6 undulator. It exhibits a sufficiently large overlap between the 1st and 3rd harmonic, allowing to finish Fe EXAFS on the 1st harmonic and to start Co or heavier 3d metal K-edge XAFS with almost closed gap on the 3rd harmonic.

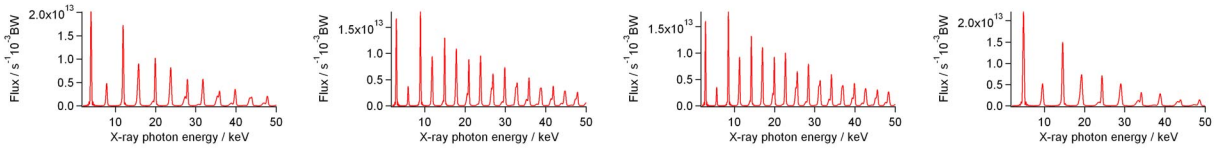

Figure 33: Expected flux through a 1 x 2 mm^2 aperture at a distance of 60 m from a short (12 periods) U32.0 undulator. From left to right K = 1.867(1st harm. at 4000 eV), K = 2.306 (3rd harm. at 9000 eV, 5th harm. at 15000 eV), K= 2.384 (5th harm. at 20000 eV), K = 1.578 (9th harm. at 44000 eV)

For an EXAFS beamline the flux through a reasonable aperture is usually more interesting than the brilliance. The expected flux through an aperture of 1 x 2 mm^2 (v x h) at a distance of 60 m (Sample position) is shown in figure 33. Table 12 summarises the parameters used for the calculation of the flux. The flux was calculated using the SPECTRA code in version 9.1 (Tanaka & Kitamura, 2001). The photon flux produced by the 1st, 3rd and 5th harmonic is between 1 and 2.5 $\cdot$ 10^{12} s^{-1} into 10^{-3} bandwidth. One can therefore expect a flux of $\sim 10^{11}\,s^{-1}$ for the monochromatic beam (10^{-4} BW) behind a Si(111) DCM. This is about one order of magnitude more than at the existing DORIS III EXAFS beamlines. The spot size at the sample position is comparable to the present beamlines.

4.4 Ray tracing results

Ray tracing results are calculated using the set-up summarised in Table 13. It shows the components and parameters which as they were included in the ray tracing calculations. All

Table 12: Key parameter of the U32.0 undulator

Parameter	**Value**
Storage ring energy	6.08 GeV
Max K value	2.6
Period length	32 mm
Length / Number of periods	38.5 cm / 12 periods
Minimum magnetic gap	10.05 mm (9.5 mm)
Integral power (@ K = 2.6 and 100 mA)	680 W

positions and distances are only approximate. The results are however largely independent of the exact positions of the optical components, because of the small divergence of the source and because of the fact that only plane reflecting surfaces are involved.

The aperture (1 σ) of the central cone of the 1$^{\mathrm{st}}$, 3$^{\mathbf{rd}}$ and 5$^{\mathbf{th}}$ harmonic of a 12 period undulator at K = 1.867 (corresponding to 4000 eV, 12000 eV and 20000 eV) is 0.028, 0.016 and 0.013 mrad, respectively.

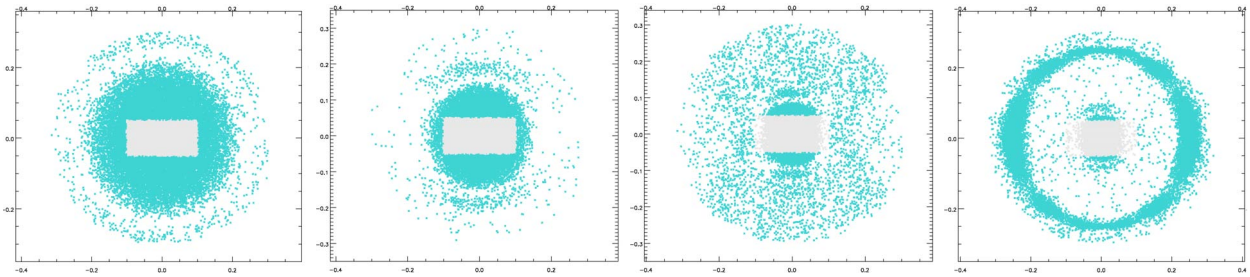

Figure 34: Central part of the undulator beam at the sample position in 60 m distance from the source, from left to right 4000 eV 1$^{\mathrm{st}}$ harmonic, 9000 eV 3$^{\mathrm{rd}}$ harmonic, 25000 eV 7$^{\mathrm{th}}$ harmonic, 44 keV 9$^{\mathrm{th}}$ harmonic, parameters are found in table 13, the brighter rectangles in the centre contain the respective parts of the beams that pass through the final $1 \cdot 1$ mm^2 slit and hit the sample. Note that in case of the higher harmonics the diameter of the central cone is smaller than 2 mm.

Figure 34 shows the foot prints of the beam emitted by the 12 period undulator tuned to 4000 eV (K=1.867, 1$^{\mathrm{st}}$harm.), 9000 eV (K=2.306 3$^{\mathrm{rd}}$harm.), 25000 eV (K=2.384 7$^{\mathrm{th}}$harm.) and 44000 eV (K=1.578 9$^{\mathrm{th}}$harm.) on the sample. In case of the harmonics larger 5 the 2 mm wide monochromator entrance slit is already larger than the 1σ width of the central cone. This will result in a pronounced horizontal intensity profile in the beam and it limits the maximum beamsize to $1 \cdot 1$ mm^2 at higher energies.

Table 13: Parameter used for ray-tracing calculations, the calculations were done for a mirror-DCM-mirror set-up. The results for a mirror-mirror-DCM set-up would be similar

Distance from source	**Component**	**Properties**
0 m	Source	12 period undulator, λ_U= 32 mm, K_{max} = 2.6, tuned to resp. energy, Max. divergence 0.05 mrad
49 m	Entrance slit	$2 \cdot 1$ mm^2
49.5 m	Optional C filter	Cooled, thickness 0.5 , 1 or 2 mm, used above 20 keV
50 m	1st mirror	Plane, 3 stripes, cooled
51 m	Diamond window	thickness: 20 μm, diameter: 4 mm
51.5 m	1st crystal	Si(111) or Si(311), $4 \cdot 4$ cm^2
51.6 m	2nd crystal	Si(111) or Si(311), $4 \cdot 4$ cm^2
52.0	Diamond window	Thickness: 20 μm, diameter: 4 mm
53 m	2nd mirror	Plane, 3 stripes (Si, Rh, Pt), uncooled
59 m	Exit slit	$2 \cdot 1$ mm^2
60 m	Sample	

Table 14 summarises the photon flux values that were used to scale the results of the ray-tracing calculations shown in table 15. In the most frequently used energy range up to 25 keV the monochromatic photon flux is well above 10^{11} s^{-1}. At lower energies (below 12 keV) when the Si111 crystals are used the flux is higher than 10^{12} s^{-1}. Only at the highest energies of the working range the flux drops below 10^{11} s^{-1}, but remains still significantly larger than 10^{10} s^{-1}.

Even if the presented values are the upper limit, because they do not account for losses due to mirror roughness etc., the flux on the sample will for many years satisfy all demands of the foreseen applications at P65. That means, in contrary to an alternative beamline design without a cooled mirror in front of the water-cooled DCM which is therefore limited to a shorter (5 periods) undulator, this set-up is competitive for many years without the need of an early upgrade with a longer undulator and a cryogenically cooled high heat load DCM.

Table 14: Flux from a U32.0 undulator into 10^{-3} bandwidth and 0.05 mrad divergence, storage ring current 100 mA, these values were used to scale the ray-tracing results

E / eV	**Harmonic**	**K**	**Flux / s^{-1}**
4000	1^{st}	1.867	$4.68 \cdot 10^{13}$
9000	3^{rd}	2.306	$2.79 \cdot 10^{13}$
15000	5^{th}	2.306	$1.61 \cdot 10^{13}$
25000	7^{th}	2.036	$7.57 \cdot 10^{12}$
44000	9^{th}	1.578	$1.29 \cdot 10^{12}$

Table 15: Calculated monochromatic flux on sample for different DCM configurations, calculated for U32.0 with 12 periods, slit size 1·2 mm^2, 20 μm thick C-windows in front of the DCM and behind the 2^{nd} mirror.

E / eV	**Crystal**	**Mirror**	**C-filter**	**Flux / $10^{11}s^{-1}$**	**FWHM / eV**
4000	Si(111)	Si 4 mrad	-	17	0.50
9000	Si(111)	Si 2 mrad	-	31	1.25
15000	Si(311)	Rh 2 mrad	0.5 mm	4.0	1.24
25000	Si(311)	Pt 1.5 mrad	2 mm	1.8	2.72
44000	Si(311)	Pt 1.5 mrad	2 mm	0.24	7.5

4.5 Experimental hutch

Figure 35 shows a ground-plan of the experimental hutch. It will have a size of approximately $4 \cdot 6$ m^2, which is comparable to the hutch of beamline C at DORIS III. The height is limited by the overhead crane and must not exceed 4.5 m including all tubes etc. installed on the roof of the experimental hutch. This results in a height of the ceiling of the hutch of 4 m. This is high enough to mount for instance a He-transfer tube in the standard dewar bottles for liquid helium. Access to the hutch is possible via a 1.6 m wide sliding door at the end of the hutch (see Figure 36).

In the lateral direction the distance between the beam and the wall of the experimental hutch will be 1 m on the left hand side (looking downstream) and 3 m on the right hand side. The limit on the left side is set by the beam pipe of beamline P64 which must be outside of P65's experimental hutch to allow completely independent operation of both beamlines.

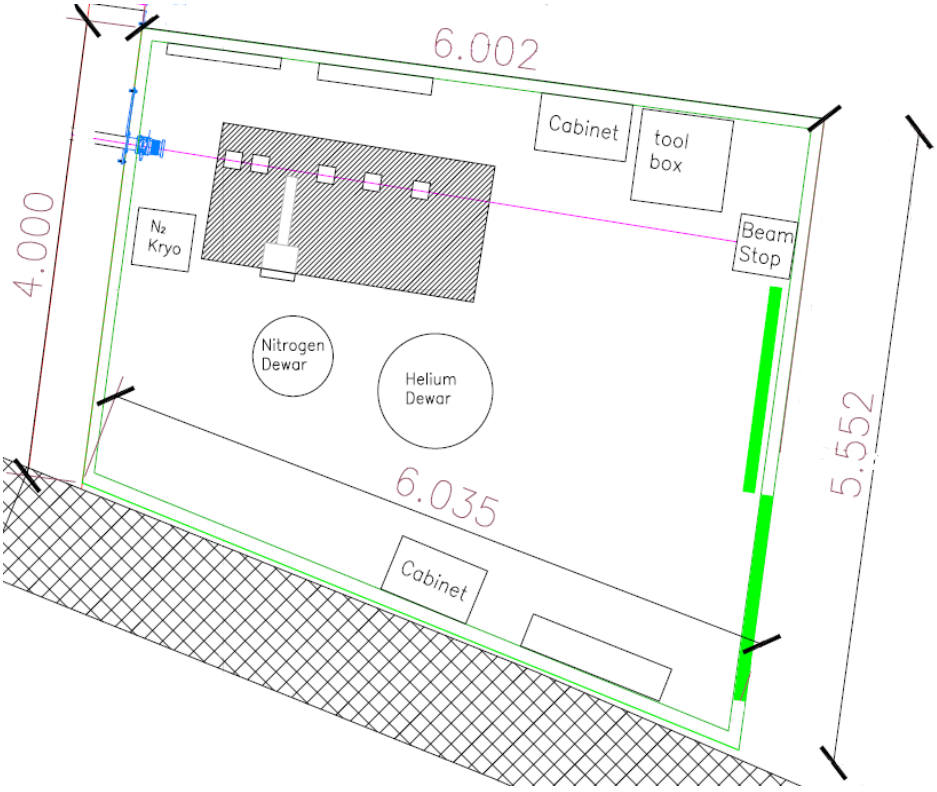

Figure 35: Ground-plan of the experimental hutch of beamline P65

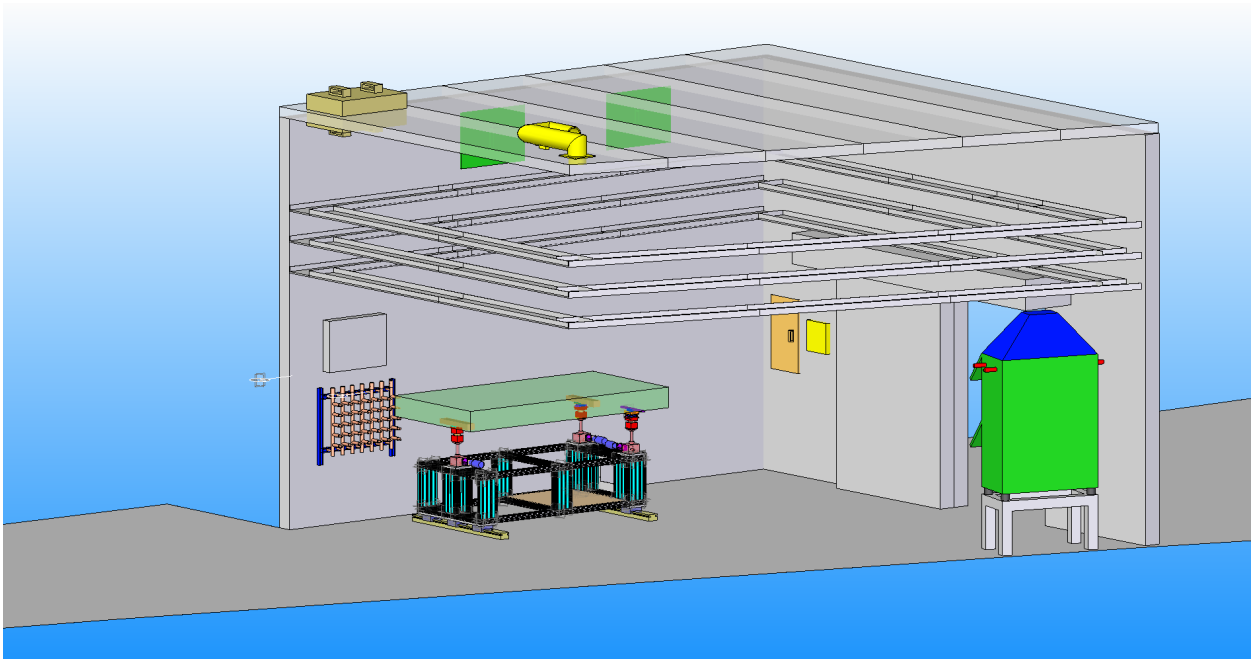

Figure 36: CAD drawing of the experimental hutch of beamline P65

4.5.1 Experimental table

The experimental table will have a size of $1.2 \cdot 2.5$ m^2 It is foreseen to re-use the complete experimental table (breadboard and height adjustable pillars) which is currently installed

at the DORIS III beamline C. Figure 37 shows a photograph of this set-up. The complete vacuum tube including the standard sample holder is removable within less than 15 min. After removing the vacuum tube user equipment like ovens, cryostats or in-situ cells of all kinds can easily be installed on the table. Minor modifications and improvements of the approved design will include arrangements to achieve a more reproducible position of the sample holder after re-installation of the vacuum tube.

Figure 37: Photograph of the experimental table at DORIS III beamline C.

4.5.2 Gas supply

Gas lines and gas storage cabinets for He, N_2, Ar and Kr are necessary for the operation of the ionisation chambers. At least He and N_2 will permanently be available in larger quantities, because they are regularly used for flushing or filling sample chambers etc. In-situ experiments require gases which are toxic, inflammable, corrosive etc. Mixtures of these gases must be avoided under all circumstances. It is therefore necessary to install a sufficient number of independent gas lines from the storage cabinets to the experimental hutch. The gas supply infrastructure at beamline X1 at DORIS III can in general be seen as a 'blueprint'

for beamline P65. 2 or 3 additional gas lines are nevertheless deemed to be necessary by the users of that beamline.

4.5.3 Other media

Cooling water and pressurised air will be available in the hutch.

4.6 Detectors

The beamline will use ionisation chambers for transmission measurements and different energy dispersive detectors for fluorescence yield XAFS.

4.6.1 Ionisation chambers

Using a 12 period mini undulator without focusing optics results in a flux and flux density which are about 1 order of magnitude higher than the respective values at the DORIS III XAFS beamlines. Tests with the existing ionisation chambers at PETRA III undulator beamlines at even higher flux densities suggest that the ionisation chambers can be used at P65 without saturation effects.

These ionisation chambers have a length of 10 cm, and a window size of $4 \cdot 6$ mm^2. The window material is 8, 25 or 50 μm thick polyimide (Kapton) foil. The pressure of the gas inside the chamber is variable between 35 and 1000 mbar. At DORIS III beamlines they are operated at 300 V - 400 V bias voltage. The bias voltage can be increased to more than 1 kV if necessary to avoid saturation effects. In that case the minimum pressure especially for Ar filling must be increased. High voltage supplies (ISEG XYZ) can be re-used form the DORIS III EXAFS beamlines.

Keithley 428 current amplifiers will be used to measure the current in the ionisation chamber. They can be re-used form the DORIS III XAFS beamlines. The analogue output of the KEITHLEY 428 will be digitized using VME VFCADC modules. They offer a linear input working range between 0 to +10 V.

An addition to the existing systems will be an automated re-fill and gas change system that is currently designed. It will alleviate user operation and protect the current amplifiers.

4.6.2 Fluorescence detectors

The beamline will need several different detectors for the detection of fluorescence yield XAFS. These detectors are part of the beamline infrastructure and should – because of their

frequent use – not be part of a larger detector pool. The field of energy dispersive detectors is currently rapidly evolving, so that it seems reasonable to postpone a definitive decision about the type of detector. Today multipixel SDD became more and more popular at EXAFS beamlines, because of the high maximum count rates, their good energy resolution, small form factor and robust operation without cryogenic cooling. Their main disadvantage is their rapidly decreasing efficiency at E $>$ 15 keV. For this energy range a multi-pixel HPGe detector is a technically most attractive alternative. In addition to the energy dispersive detectors relatively inexpensive and robust detectors for total fluorescence detection like PIPS diodes or modified Lytle detectors will be used.

5 Common sample preparation labs

We require a total of three lab rooms for the two EXAFS-beamlines P64/P65. One lab, shown in figure 38 will be installed between the two beamlines (see Figure 3) close to the experimental hutches for sample preparation and sample treatment. This set-up has been proven to be very successful in the case of beamline X at DORIS III. Major equipment of this lab includes a fume-hood for toxic and harmful gases, a bench for wet-chemistry, a glove-box, and lockable cabinets to store all kinds of chemicals during their use in the laboratory. Like at X1 the preparation lab will also contain smaller equipment like an analytical balance and a hydraulic press for pellet preparation.

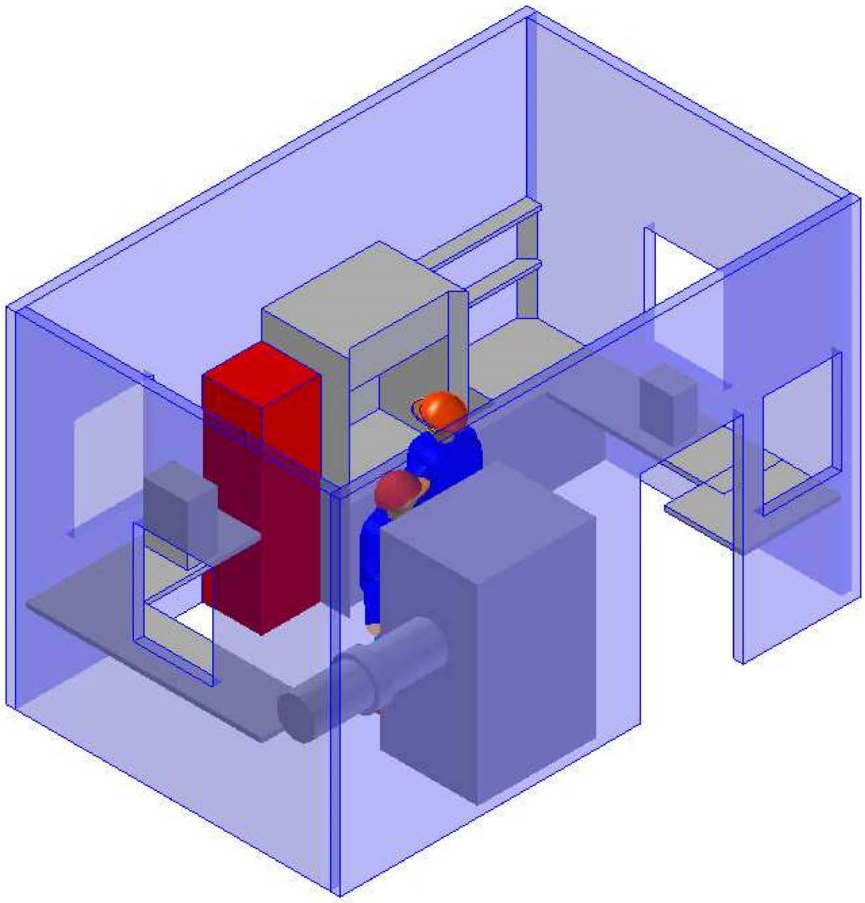

Figure 38: Preparation lab for beamlines P64 and P65

A second small lab is required for sample preparation and offline sample characterisation by the Bio-XAS users and is also funded within a corresponding BMBF-project. A third lab is required for storage, maintenance, and repair of beamline equipment, which is not in use at the beamlines. This lab needs not to be close to the beamline, but it should be in the same building. The main equipment will be tools and workshop equipment.

6 Timeline

The timeline for the beamline design and construction is intemately interleaved with the overall time schedule of the PETRA III extension project which is very ambitious in terms of total construction time. According to the current planning, the mandatory PETRA III shutdown will start on May 13, 2013. The reconstruction of the storage ring inside the existing ring tunnel as well as the civil engineering work outside the tunnel will be parallel to large extent. The commissioning of the reconstructed storage ring is planned to start in October 2013. In order for the machine to be able to operate, all radiation shielding in the two new experimental halls has to be completed.

XAFS beamlines P64 and P65 are planned to be the first two beamlines becoming operational at the PETRA III extension. The beamline construction strongly depends on various strict boundary conditions given by progress of the civil engineering of the experimental hall and installation of the beamline frontend components. Note, that the installation of basic technical infrastructure (electricity, water, air conditioning etc) in the new experimental hall will continue while the storage ring is again operated for experiments at beamlines P01-P14. The installation of optics and experiments hutches for the new beamlines will start even before the installation of the technical infrastructure in the halls. Access to the frontend area is needed to install the insertion devices and remaining beamline components of P64 and P65. This will require an extended machine shutdown which has to be kept as short as possible as well as scheduled well in advance. A machine shutdown is tentatively scheduled for April/May 2014 and will be used to complete P64 and P65. It is planned to provide first beam at both beamlines for (friendly) user groups in late summer of 2014, depending on the machine operation schedule in that period (details to be decided later).

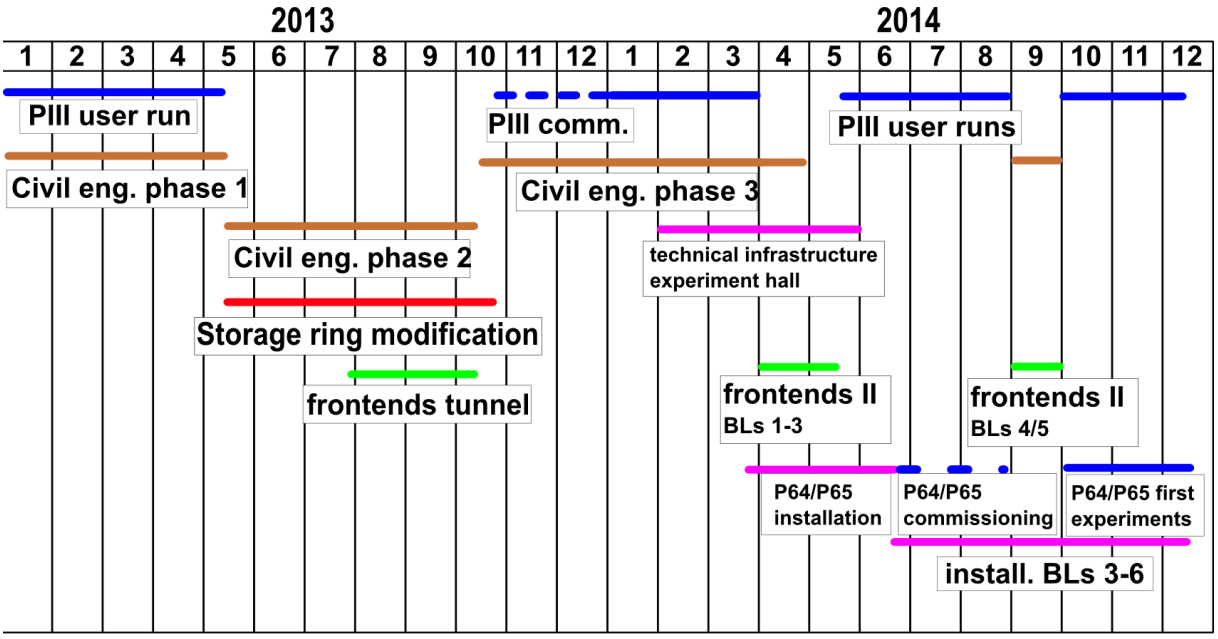

Figure 39: Schematic Extension Project Timeline

06.2012 start conceptional magnet design of undulator	FS-US
11.2012 call for tender for undulator support structure	FS-US
11.2012 call for tender for mirrors	FS-BT
11.2012 call for tender for undulator magnet structure	FS-US
12.2012 place order for monochromator	FS-BT
03.2013 place order for hutches	FS-TI
08.2013 install front-end tunnel components	FS-BT
01.2014 build optics hutch	external company
02.2014 start to build beamline starting from optics hutch	FS-BT
02.2014 build experimental hutch	external company
04.2014 set-up experiment in experimental hutch	beamline staff
04.2014 install undulator	FS-US
04.2014 install front-end II components	FS-BT
06.2014 wire-up beamline and check all motors and electronics	beamline staff
07.2014 start commission beamline	beamline staff
10.2014 first experiments (friendly users)	
02.2015 commission spectrometer	depends on external funding

References

Chubar, O. & Elleaume, P. (1998). *proc. of the EPAC98 Conference, 22-26 June 1998*, pp. 1177 – 1179.

del Rio, M.S., Dejus, R. J., XOP Home page: http://www.esrf.fr/computing/scientific/xop2.3/

Franz, H., Leupold, O., Röhlsberger, R., Roth, S.V., Seeck, O.H. ,Spengler, J. , Strempfer, J., Tischer, M., Viefhaus, J., Weckert, E., Wroblewski, T. (2006) *Synchr. Rad. News* **19**, 25 – 29.

Rickers, K., Brüggmann, U., Drube, W., Herrmann, M., Heuer, J., Welter, E., Schulte-Schrepping, H., Schulz-Ritter, H. (2007). *AIP Conf. Proc.* **879**, 10.1063/1.2436208.

Sanchez del Rio, M. & Dejus, R. J., (1997). *SPIE Proc.* **3152**, 148–150.

Tanaka, T. & Kitamura, H. (2001). *J. Syn. Rad.* **8**, 1221–1228.

Wellenreuther, G. (2012). Personal communication.

Welter, E. (2010). *AIP Conf. Proc.* **1234**, DOI:10.1063/1.3463376.